Eidgenössische Technische Hochschule Zürich
Swiss Federal Institute of Technology Zurich

Master Thesis

MICROSCALE 3D PRINTING OF MULTI-METAL IN MENISCUS-CONFINED ELECTRODEPOSITION

Albert Ripoll Oliveras

Supervisors

Dr. Dmitry Momotenko

Julian Hengsteler

Professor

Prof. Dr. Janos Vörös

Zürich, October 2020

"Out of clutter, find simplicity. From discord, find harmony.
In the middle of difficulty lies opportunity."

- Albert Einstein

Abstract

Additive manufacturing (AM) has transformed the way we can design and produce components at the macroscale level. AM has enabled the fabrication of innovative products with specific geometries that are not accessible by traditional manufacturing techniques. Microscale AM holds a great potential in a broad range of scientific applications. However the downscaling of additive techniques to the micro- and nanoscale is still in state of art when it comes to metal printing. The exploration of the new submicrometric AM comprises the multi-material capabilities. The extension of the chemical control composition to the metal AM has been found to be a strongly promising field of analysis as several applications and techniques are arising.

Herein, a microscale multi-metal AM technique based on the meniscus-confined electrodeposition (MCED) is introduced. This multi-metal novel technique enables the direct printing of individual and mixing of multiple metals from a single multichannel nozzle. Multi-metal MCED combines the high spatial resolution of MCED printing, with the in situ straight-forward deposition of metal ions from metal salt solutions. This technique unlocks a simple way to 3D print multi-metal structures with pre-defined local properties and opens new pathways for the direct fabrication of materials and devices with unique chemical architectures.

Moreover, a study of several feasible substrate materials for MCED and a system for printed features damage-free release from the substrate are elaborated. The releasing methodology enables the confinement of the structures in a reduced area for continuous visual tracking.

Acknowledgements

First and foremost, I would like to express my deep gratitude to my main supervisor Dr. Dmitry Momotenko for his insightful guidance, support and inspiration, which made this project possible. Thanks to his advice and mentoring, this stage at ETH Zürich has been a constant learning. It has been a pleasure meeting him both, professionally and personally.

Second, I would like to thank Prof. Janos Vörös for providing me the opportunity to be part of the Laboratory of Biosensors and Bioelectronics (LBB) and to close my master studies with a unique research experience at ETH Zürich. Next, I am grateful to the whole LBB, all of its students and employees, for creating a comfortable, warm and friendly environment. I have plenty of great memories of these last months despite the rare situation that we have gone through all this year.

I would also like to thank Julian Hengsteler for his tireless help during the project and his demonstration of perseverance when adverse results were obtained. I am grateful for not only all the visits he has done to Hönggerberg campus for sample's imaging or substrate manufacturing, but also for the discussions and the innovative ideas he was always proposing for the research.

Most importantly, I am thankful to my family. Despite being hundreds of kilometers away, they have been always here, by my side, supporting me and offering me advice whenever I needed it. Especially to my parents, for their support and unconditional love. Without them, all this would not have been impossible. Moltíssimes gràcies!

Table of contents

List of Figures

List of Tables

1. Introduction

Additive manufacturing (AM) has transformed the way we can design and produce components at the macroscale level. AM has enabled the fabrication of innovative products with specific geometries that are not accessible by traditional manufacturing techniques such as machining, molding or forging. The traditional techniques are often call for subtractive methodologies and call for an easy manufacturing geometry and limit to non-ideal geometries. However, AM can implement the geometry required for best performance freeing the design from restrictions imposed by classical fabrication. An exceptionally broad range of applications emerge from AM, in different fields but also in different size scales. AM is used from printing buildings [1] and in the aviation and automotive industry [2, 3] to bioprinting of tissue [4] and micro- and nanometric electronics [5].

Whereas AM in macroscale is already being commercialized, there's a lot to be done in micro- nanoscale. Currently, most of the traditional microfabrication methods are planar (2D) and not well suited for the fabrication of complex three-dimensional (3D) parts. Since the additive approach of AM overcomes the 3D limitations, it will be a valuable addition to traditional microfabrication methods. Microscale AM holds a great potential in a broad range fields and applications such as sensors [6], optics and photonics [7], microelectronics [8], quantum computing [9], biotechnology and biomedicine [10], and metamaterials [11, 12]. However the downscaling of additive techniques to the micro- and nanoscale is still in state of the art when it comes to template-free metal printing. Various techniques have emerged that are currently under development and in prototype stage, its full potential is still to be explored.

The exploration of the new submicrometric AM comprises the multi-material capabilities. The extension of the chemical control composition to the metal AM has been found to be a strongly promising field of analysis as several applications are arising such as manufacturing batteries [13, 14], thermocouples [15], biomaterial metamaterials [16], and materials with locally tailored electrical resistance [17], chemical reactivity [18] or microstructures [19]. We are not even in the beginning of the multi-material fabrication and the full potential of this AM has still to be seen. At present, the multi-material techniques have two main limitations that need to be overcome. First, the usual multi-nozzle approaches limit a lot the 3D structure for complex geometries and lack of geometrical precision. Second, most techniques employ nanoparticle inks that are often chemically behind of the microfabrication demands and require complex post-printing processes. These two limitations and other technical difficulties make multi-material microfabrication in 3D AM an incredible

challenge. The existing techniques are truly scarce and only few examples have been shown. None of them, until the date, using electrochemical methods.

Here, we develop and introduce a microscale multi-metal AM technique based on the meniscus-confined electrodeposition (MCED) [20, 21, 22]. We explore new potential practices for the MCED. This multi-metal novel technique overcomes the previous limitations of micro and nanoscale multi-material AM for the case of metals deposition, as it enables the direct printing and mixing of multiple metals from a single nozzle. Multi-metal MCED combines the high spatial resolution of MCED printing, with the in situ deposition of metal ions from metal salt solutions. We demonstrate that the combination of submicron geometrical structure size and fast control of the chemical composition offers unmatched control of the 3D chemical architecture of printed parts and enables tuning of local properties through local alloying at the submicron scale and multi-metal interactions. Moreover, we elaborate a system for printed structures damage-free release from the substrate confining them in a reduced area for continuous visual tracking.

1.1. State of the Art

Over the years extensive research has been done on microscale 3D AM. For polymeric materials, great progress has come from the ascent and establishment of micro-stereolitography (MSL). MSL also known as direct laser writing or two-photon polymerization is a technique that enables the creation of small features in a photosensitive material without the use of complex optical systems or photomasks [23, 24]. The method is based on a multiphoton absorption process in a transparent material at the wavelength of the laser used for creating the part. By scanning and correctly modulating the laser, a chemical change (usually polymerization) occurs at the focal position and can be controlled to create 3D pattern. Recently it has been shown that combining MSL and thermal treatments, AM of 3D glass-ceramics can be achieved [25]. There are several application fields for microdevices made by MSL such as biomedical engineering [26], microfluidics [27], optics [28], etc. However, this technique is limited to photoresist materials. There are many other applications that require the use of conductors or semiconductors materials such as in sensing, microelectromechanical systems, medical implants or electronics. MSL can be used to create templates for later metallization by coating or templated electrodeposition [29, 30] but no mask-free metal AM technique has been established for the microscale.

Consequently, ongoing research focus to develop ways for metal AM at microscale. Some of these existing approaches for AM of metal structures are presented and a mention to the materials that have been demonstrated for good operation is given [31].

Direct ink writing (DIW) of metals is based on the extrusion of concentrated metal nanoparticle inks from micrometer-sized nozzles. An overpressure is applied causing an ink filament to exit the nozzle. The ink consists of highly concentrated silver nanoparticles coated with poly-(acrylic acid) dispersed in water and ethylene glycol. A post-deposition annealing is needed. It can be done thermally [32] or using an in situ annealing laser system [17]. The second systems provides more versatility in the substrate choice. So far, DIW for metals has solely been used with silver nanoparticles.

Electrohydrodynamic printing (EHD) is a method based on the electrohydrodynamic ejection of an ink jet or individual ink droplets from a nozzle. A voltage of 100-1000V is applied between the capillary and the substrate to initiate printing. Driven by the electric field, the mobile ions or charged particles in the solvent meniscus migrate to the solvent-air interface. Due to electrostatic repulsion between ions, the surface tension of the solvent is overcome and a jet or a droplet is ejected towards the substrate. The ejection frequency can be controlled by the pulse frequency when a pulsed field is used instead of a constant electric field where the frequency depends on the applied voltage. When the droplet lands on the substrate, the solvent is evaporated and a well-defined deposit is obtained. Given that all of the solvent evaporates faster than the droplets frequency, the deposits can be stacked to build 3D structures [33, 34]. Gold and silver nanoparticles are commonly used with this technique. In addition, copper, cobalt and aluminum have been proved to work. A sequential use of different nozzles filled with different inks enables the deposition of multiple materials [35].

Local electrophoretic deposition is a technique that combines the optical trapping of nanoparticles with the electrophoretic deposition because of the influence of an electric field [36]. A focused laser beam is directed into a suspension of charged metallic nanoparticles and optically traps and accumulates them in its focal spot. In addition, a constant electric field is established across the suspension and forces the particles to coagulate and settle on the substrate. By leading appropriately the particles with the laser, they can be assembled into 3D structures. So far, this method has only been demonstrated with gold nanoparticles.

Laser-induced forward transfer (LIFT) technique is based in the direct transfer of various materials by ablation. A focused laser is employed to induce local melting of a thin metal film (donor) coated onto a glass slide (carrier). When the metal melts, a liquid metal droplet is transferred to the substrate located right below the carrier. Upon impact, the droplet quickly solidifies. Subsequently, the carrier moves laterally to expose a new region of the metal film to be melted for the next droplet. With the correct relative movement of the substrate and the carrier, 3D structures can be built through stacking the metal droplets [37, 38, 39]. Several metals have been used with this technique including aluminum, copper, gold

and metal alloys. Multi-material printing can be performed using a carrier containing donors of different materials [40].

Laser-induced photoreduction is able to induce local photochemical reduction of metal salt solution upon laser irradiation. The metal salt solutions can be aqueous [41] or non-aqueous [42] of $AgNO_3$ or $HAuCl_4$, often containing additional photosensitizing dyes and sacrificial donors. A localized photoreduction is consummated in the laser focal spot which movement in three dimensions enables the creation of 3D metal structures. The electrons required for photoreduction are usually excited in the dye molecules and afterwards transferred to the metal ions. As soon as the reduction takes place, nucleation and growth of metallic crystallites in solution or on a surface initiates. After an electron transfer, the neutral state of the dye is restored by the sacrificial donor [43]. Studies of this technique are almost exclusively on deposition of silver structures but additional reports of gold and copper deposition exist.

Focused electron/ion beam induced deposition (FEBID/FIBID) involves the decomposition of gaseous molecules (precursor) by an ion/electron beam with a subsequent solid deposition of non-volatile dissociation products onto a nearby substrate [42]. Precursors for a wide range of metallic materials are available. However some of them do not achieve the deposition of a pure metal. Some demonstrated metals deposited are Al, Au, Co, Cr, Cu, Fe, Pt, Ti and Sn [44, 45]. The synthesis of binary systems such as Pt-Si, Co-Si, Co-Pt and Fe-Si is possible if separate gas injection systems are available for each precursor [46, 47, 48].

Electroplating of locally dispensed ions in liquid relies on the use a hollow AFM tip called FluidFM cantilever immersed in an electrolyte bath for deliver very localized metallic ions. The metal ions are only present in the pipette and the localized supply is achieved through the nanosized pipette aperture. The pipette is approached to a cathodically polarized substrate and a controlled dispensing of metal ions is induced from the aperture. The ions exiting are electrochemically reduced and deposited on the substrate. The growth of the deposit is detected by a feedback mechanism that maintain a constant separation between the aperture and the structure [49]. The methodology has only been used for 3D deposition of copper.

Meniscus-confined electrodeposition (MCED) technique is based in the use of nanopipettes. A nanopipette filled with a metal salt solution is approached to a conductive substrate. Due to the suspended droplet at the pipette tip, a liquid meniscus is formed when it is close enough to the substrate. Electrochemical reduction of the metal ions is triggered because of the negatively polarized substrate versus a counter electrode placed in the pipette.

The controlled retraction of the pipette promotes the 3D growth of the metal structure [50]. The technique has been used for copper, platinum and silver [20, 21].

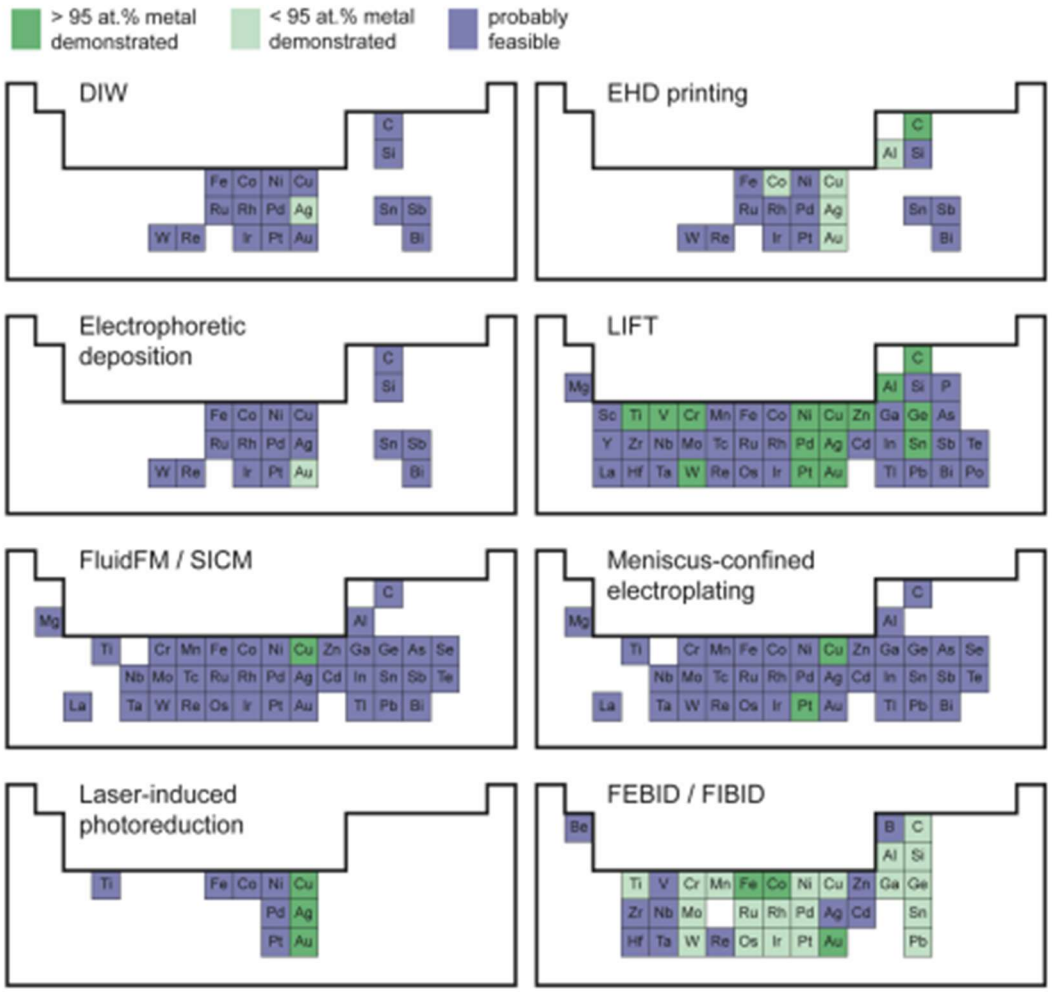

Figure 1-1. *Periodic tables showing the elements that have been deposited with the respective technique. Dark green squares represent pure deposits whereas light green squares indicate that the as-deposited materials were metal-organic composites. Blue squares denote elements we assume could be deposited with the technique. Figure obtained from L. Hirt, A. Reiser, R. Spolenak and T. Zambelli [*31*].*

Only few techniques between the previously presented are shown to support multi-material printing. Some of them require several subsequent approaches or multiple nozzles (LIFT, EHD), others require adding more complex accessories to the setup (FEBID) or are limited to metal-polymer composites (Laser-Induced photoreductor). Two of them are able to print alloys (LIFT and EHD) but the other two only systems of several metals (FEBID and Laser-Induced photoreductor) with a limited level of purity.

1.2. Contribution and Project Overview

Metal AM at submicrometer scale is at the AM research spotlight. A multitude of techniques that allow 3D fabrication of metals are being studied and developed currently. For this project, MCED technique is employed and improved. MCED offers various advantages compared to other AM methods. This technique seems to be the simplest and most affordable of all the previously presented. The process takes place in open air without any requirement on environment or infrastructure is needed. There is no need for a cleanroom, ultrahigh-vacuum or other complex systems that require a lot of money to maintain. The instrumentation required is pretty simple as it is based on electrochemical equipment and any Focused Ion Beam (FIB), Scanning Electron Microscope (SEM) or complex optical system (Lasers) is needed. Moreover, the nozzle is fabricated using pipette pulling techniques which is simple, fast (few seconds), cheap (less than a dollar per nozzle), reproducible and capable to tune nozzle aperture and to reach aperture diameters approaching single nanometer scale. Finally, as seen in Figure 1-1, the amount of possible printed materials with MCED is substantially larger than most of the other techniques.

Chemical composition control in multi-material AM printing at micro and nanoscale is a novel practice as it is being developed while the already existing submicrometer AM techniques are further studied. Different approaches to achieve the same objective are currently flourishing.

In this project we develop a new multi-metal technique evolved from MCED. The study introduces the use of multi-barrel pipettes for multi-material MCED. Until now, this type of pipettes were only used in MCED setups for more precision and feedback while printing [51, 52] or for parallel structures printing [53]. In 2019, Reiser A. et al. [54] developed an AM technique for multi-metal submicron scale based also in the use of multi-barrel pipettes with a completely different methodology (EHD redox printing).

The developed technique enables to print any pair of metals that MCED permits through a single nozzle and with a deep control in the chemical composition of the deposition. The project encompass the finding and defining all the critical parameters for the correct operation of the multi-metal technique. Subsequently, we implement and optimize the printing of three new metals (Cu, Pt and Au) in the MCED. Afterwards, we put into effect these metals in the multi-metal MCED to test its correct performance. And, finally, we elaborate a system for printed structures damage-free release from the substrate confining them in a reduced area for continuous visual tracking.

2. Theoretical foundations

In this chapter, some theoretical concepts and the basics of the MCED printing method are going to be defined.

2.1. Introduction to Meniscus-Confined Printing

MCED printing uses localized electroplating to build the desired metallic structures. A localized electroplating is achieved thanks to the employment of glass pipettes with nanometric aperture filled with electrolyte. A liquid meniscus is created between the pipette tip and the substrate. In this way, the electroplating process only takes place in a specific point on the substrate where the meniscus is formed. Different metallic features can be printed by the reduction of metal ions present in the electrolyte.

2.1.1. Electroplating basics

Understanding the fundamental mechanism in which the MCED printing is based is extremely important. This is why in this chapter some electrochemistry and electroplating principles are going to be defined.

Electroplating is a widely used technique in industry and research in which a metal coating is created on a solid substrate. The coating is achieved through the reduction of cations of the desired metal on the substrate (see equation 1). This technique is industrially used to improve surface qualities such as resistance to abrasion and corrosion, reflectivity, appearance, electrical conductivity, magnetic layers or others [55].

$$M^{z+} + z\, e^{-} \leftrightarrow M \tag{1}$$

The reduction of metal ions M^{z+} can be accomplished by two different processes: an electrodeposition process in which z electrons are provided by an external power supply, and an electroless (autocatalytic) deposition process in which a reducing agent in the solution is the electron source (no external power supply involved). [56] In this project, the first method is the one that applies.

An electrochemical cell for electrodeposition consists usually of three components: two electrodes (a cathode and an anode) and an electrolyte (often a reference electrode is needed). In the case of an electrolytic cell for electroplating, the electrolyte is usually a solution of

water or other solvents with dissolved ions of the metal to be deposited. The cathode (negative electrode) is where the reduction of cations takes place and, therefore, is the part that is coated. The anode (positive electrode) is usually an inert conductive material or a block of the same metal that is being used for coating in order to replenish the electrolyte ions that have already been plated out. Finally, an external electrical potential is applied in order to overcome the reversible cell potential and produce the chemical reaction which would not occur spontaneously. A schematic diagram of a traditional electroplating system is shown in Figure 2-1. It is the same as a galvanic cell acting in reverse.

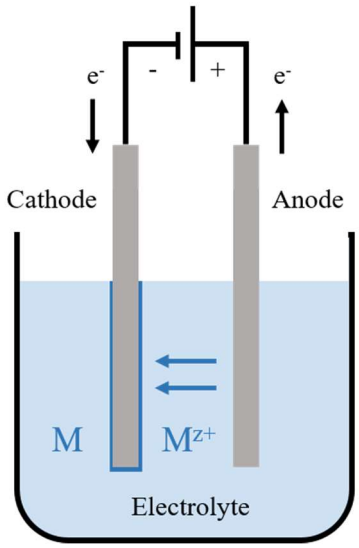

Figure 2-1. *Schematic drawing of an electrolytic cell for electrodeposition of metal M. In this example, the anode is not of the same metal as M, therefore, the M ions are not going to be replenish once they have been deposited.*

The cell potential (or electromotive force) is the potential difference between the two electrodes. To measure the spontaneity of a reaction, the Gibbs free energy is used. If the free energy is positive, the process is not spontaneous and the cell is an electrolytic cell, if the free energy is negative, then the process is spontaneous and it is a galvanic cell.

$$\Delta G = -n \cdot F \cdot E_{cell} \tag{2}$$

Where F is the Faraday constant, n the number of electrons involved and E_{cell} the cell potential. This last one is different for every reaction and for every voltaic cell. It depends on the concentrations of the reactants and products as well as the temperature and other factors. So, a standard cell potential is defined when the reaction occurs at 25 ºC, 1atm in

pressure and the concentration of the reactants and products is 1M. It is measured in a galvanic cell consisting of the half-cell with the electrode to study and half-cell with the standard hydrogen electrode (SHE). Standard electrode potentials are measured relatively to the standard hydrogen electrode, which potential is defined as 0V. The standard cell potential of any cell in standard conditions can be written as the oxidation potential plus the reduction potential.

$$E^0_{cell} = E^0_{catho} - E^0_{anode} \tag{3}$$

In order to relate the standard cell potential with the reduction potential of a specific electrochemical reaction out of standard conditions the Nernst equation is used.

$$E = E^0 - \frac{R \cdot T}{n \cdot F} \cdot \ln(C_{ion}) \tag{4}$$

Where E^0 is the standard electrode potential [V], R the gas constant [J·mol^{-1}·K^{-1}], T the temperature [K], n the number of transferred electrons, F the Faraday constant [C·mol^{-1}] and C_{ion} the molar activity (concentration) of ions.

2.1.2. Meniscus-Confined Principles

The MCED methodology enables the user to work with a broad set of different metals. By combining different parameters such as the selection of electrolyte, the type of the electrodes, the potential applied, the presence of additives and so on, a large variety of metal materials can be deposited, including gold, copper, platinum silver, nickel, cobalt, tin, zinc, etc. [57] In this project the first three metals have been studied and optimized for proper printing and to illustrate the performance of the method developed (Cu, Pt and Au).

In the MCED technique, the electrodeposition of the metal takes place inside of the liquid meniscus formed between the tip of the pipette and the conductive substrate. The pipette is filled with a metal salt solution that, when it approaches the substrate, it forms a meniscus. The metal reduction takes place when the substrate is cathodically polarized (working electrode) versus the counter electrode. Therefore, the substrate acts as cathode while the electrode that is permanently in contact with the electrolyte inside the pipette acts as anode. The electrochemical reaction is laterally limited by the liquid meniscus enabling a confined active surface. The printed structures size depends mainly on the meniscus diameter and is

closely related to the pipette opening that can go up to few tenth of nanometers [58]. In Figure 2-2 a schematic picture of the electrolytic cell for the MCED technique is shown.

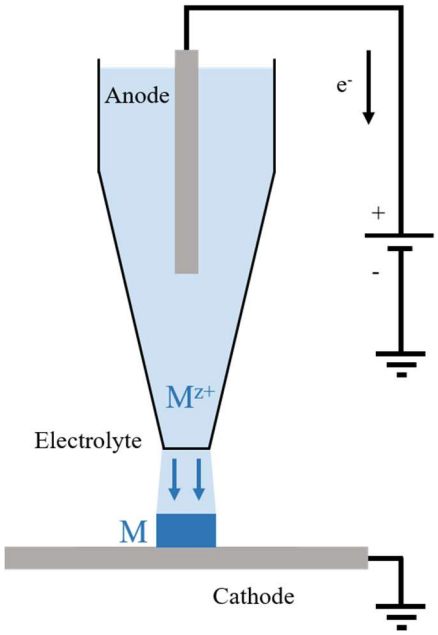

Figure 2-2. *Schematic picture of the electrolytic cell generated by the MCED technique. The cell is only complete when the meniscus is created and the circuit is closed.*

The glass pipettes are employed to deliver the electrolyte solution. A counter electrode is mounted inside the pipette, usually a metal wire, and is connected to a power supply that controls the potentials that induce the electrochemical reaction. The metal structure growing underneath the nozzle can eventually lead to aperture clogging. This will halt the growth process and will require replacement of the nozzle. To avoid this scenario, the pipette-substrate distance can be maintained by constant nozzle retraction (which is synchronized with structure growth) [20, 21, 22] or by using a feedback system [59]. In both cases, a stable meniscus that prevents pipette clotting and correct wire growing is desired. If the feedback option is implemented, a parallel voxel printing approach can be implemented [59] while with the first option, the printed wire consists of a single voxel, uninterruptedly printed. It is intrinsically hard to implement constant rate retraction at nanoscale since the rate hugely varies even with the same pipette landing onto two different locations. Therefore, the use of feedback is preferential as it allows straightforward automation of the process.

3. Fundamentals of Multi-Metal Meniscus-Confined Electrodeposition

In this project, a new MCED technique for printing two metals has been developed. The technique enables the user to print micro- and nanoscale structures with a precise control of the chemical composition which can be changed on the fly (from pure metals to arbitrary alloys). In this chapter, the multi-metal MCED technique is described. The printing system and the key parameters that rule and enable to control the technique are exposed and studied.

3.1. Multi-Metal System

The multi-metal MCED technique can be considered as an improvement of the MCED system. It uses the same principles but with some extra levels of complexity that are going to be presented below. The main difference is the use of two barrel nanopipettes (obtained from borosilicate theta capillaries). This allows to use two different electrolytes while counter-reference electrodes in each barrel allow establishing electrochemical potential on the substrate and drive ion fluxes between nozzle barrels. With the correct use of the potential in each electrode (both reference and the working electrode) and the precise electrolytes, this system opens the pathway for MCED to become multi-metal MCED.

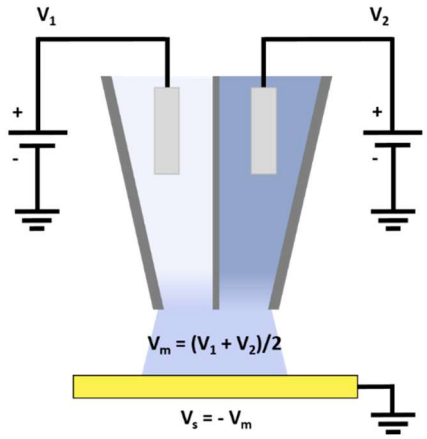

Figure 3-1. *Schematic of the electrolytic cell generated by the double barrel in multi-metal MCED technique. The cell is only complete when the meniscus is created and the circuit is closed.*

As it can be seen in Figure 3-1, the electrochemical cell for metal plating in the double barrel arrangement somehow resembles the single barrel configuration (Figure 2-2). In this case, however, the anode is composed by both reference electrodes and the cathode is the substrate

which is grounded. As in the single barrel system, the electrochemical process occurs inside the meniscus. Both barrels of the pipette are used as a local reservoir of different electrolytes that contain the metal ions. The substrate serving as cathode provides electrons to the metal ions which are transported within the meniscus. The use of different voltages (V_1 and V_2) in each barrel induces a voltage bias between the barrels which alters the transport of ions to the meniscus. This allows to control the concentration of each metal ion inside the meniscus and therefore alter chemical composition of electrodeposited metal features.

3.2. Multi-Metal Key Printing Parameters

In this chapter we are going to introduce and go further deep in the key parameters, multi-metal challenges and support techniques that are used to control the multi-metal MECD technique.

3.2.1. Double Barrel Pipettes

Micro- and nanopipettes are becoming extraordinarily versatile and powerful tools in nanoscience for a broad variety of applications from imaging [60, 61], to printing [31] and sensing [62, 63]. They allow precise spatiotemporal control, analysis, and manipulation of material fluxes. [64, 65, 66]. This is really useful for nanofabrication as filled with electrolyte can serve as reservoir of working molecules/ions for deposition and can therefore provide a highly localized flux towards the substrates [67, 68, 69, 70]. Therefore, with a precise control of pipette-to-substrate distance during deposition a high resolution can be achieved [52].

A significant attribute of nanopipette usage is the simplicity and the low cost of fabrication. Pulling capillaries with diameters that are highly tunable and range from tens of micrometers down to a few nanometers is a simple task, which does only require a laser pipette puller. This is a crucial consideration as the size of the nanopipette tip is a factor determining both, mass transport rates through the nanopipette orifice [66] and lateral dimensions of the deposit.

For multi-metal MCED pulled theta glass capillaries which contain a septum that extends the length of the pipette are used. Nanopipettes with two distinct barrels can be obtained using this type of glass capillaries [71]. The two barrels are isolated one from the other and only have contact in the tip of the pipette because of the small droplet of electrolyte that is created. This small droplet is the cause of the formation of the meniscus as soon as it gets close enough to the substrate. In Figure 3-2 a typical example of a double barrel nanopipette can be seen.

Thanks to the two independent reservoirs separated by the septum, different electrolytes and electrodes can be placed in each barrel. This enables the creation of bias between the two barrels when the respective electrodes of each barrel are connected to a different voltage (see 3.2.2). Moreover, in the contact droplet or meniscus between barrels the average between barrel's voltages is applied [51].

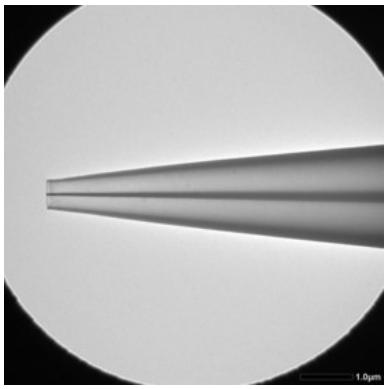

Figure 3-2. *Double barrel pipette tip TEM image with an aperture of approximately 220 nm of diameter for each barrel and a septum of 30 nm thickness.*

3.2.2. Bias between Barrels

The bias between barrels is defined as the voltage difference between the electrodes in each barrel. It is defined as the voltage in barrel one (V_1) minus the voltage in barrel two (V_2). Therefore, the bias can take positive and negative values depending on which barrel has the electrode with higher voltage.

$$bias = V_1 - V_2 \tag{5}$$

Thanks to the independent barrels of the theta pipettes, the system can store two different electrolytes in contact with independent electrodes. If the electrolytes provide the proper conductivity (see 3.2.4), the voltage in the substrate can be easily controlled. With this system, the electrodeposition (reduction) voltage of the metal can be obtained in the meniscus adjusting the two barrel voltages. The voltage at the substrate (V_s) with the electrolyte as reference is the same as the voltage in the meniscus (V_m) with inverted sign.

$$V_s = -\frac{V_1 + V_2}{2} = -V_m \tag{6}$$

Once the bias and the substrate voltage needed for the electroplating of a specific metal (see 3.2.3) are known, using equations (5) and (6), the required voltages in the two barrels (V_1 and V_2) can be calculated.

The bias between barrels is the main parameter that enables the user to have an individual management of each electrolyte deposition while printing. It permits the regulation of which metal is being electrodeposited and in which ratio. The bias and the potentials in the barrels influence the metal ions movement. The ions can be pushed towards the meniscus to induce printing but they can also be pulled away from it to reduce deposition. Depending on the polarity of the metal ion and the bias, the pulling/pushing of the ions takes place.

The way bias works can be visualized in Figure 3-3 with a simple theoretical example of a double barrel with two electrolytes. The left barrel (barrel 1) contains an inert salt solution and the right barrel (barrel 2) contains a solution with the copper ions (Cu^{2+}) that have to be electroplated on top of the substrate. Depending on the bias applied different printing situations appear.

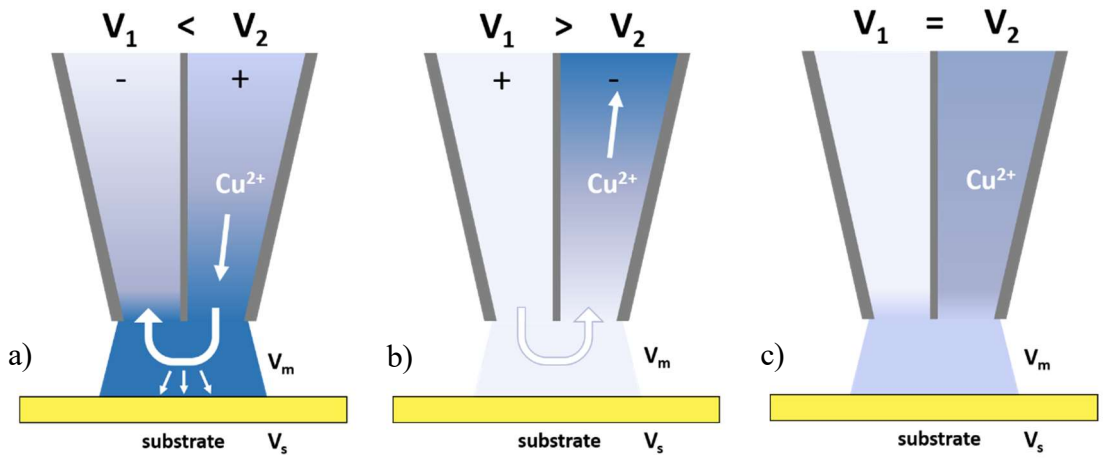

Figure 3-3. *The effect of the bias in the control of the printing electrolyte ions. Three cases are observed: a) negative bias ($V_1 < V_2$), that promotes the movement of Cu^{2+} ions onto the meniscus, pushing them towards the opposite barrel, therefore electroplating takes place; b) positive bias ($V_1 > V_2$), which attracts the Cu^{2+} ions to the electrode of the same barrel, so they are pulled away from the meniscus and the electroplating process is not possible; c) no bias ($V_1 = V_2$), so no pushing/pulling force to Cu^{2+} ions is applied between the barrels, some electrodeposition of copper can take place.*

If the specie that has to be electroplated is positively charge, such as Cu^{2+} (Figure 3-3), it is going to be attracted to the electrode with lower potential (-) and repelled from the electrode with higher potential (+). On the one hand, when the lower potential electrode is in the barrel which contains the electrolyte with the metal ion, the ions are going to be pulled away from the meniscus as they get attracted by the electrode in the same barrel (b in Figure 3-3). So the electrodeposition of the ions on the substrate is diminished. On the other hand, when the lower potential electrode is in the opposite barrel, the metal ions are pushed to the opposite barrel through the meniscus (a in Figure 3-3). This enhances the electroplating as more metal ions are pushed towards the meniscus and consequently, the substrate. If the metal ion is present in a negatively polarized form, such as $PtCl_6^{2-}$, it works the same way but with inversed attractions and repulsions to the electrodes.

3.2.2.1. Two metal arrangements for correct bias use

The system needs to be adapted in order to print two metals. Using bias, the user can control when electroplating takes place with the possibility of maintaining the desired voltage always in the substrate. Therefore, if both metals are contained in the nanopipette, with the correct arrangement, the user is able to stop the electroplating of one metal while inducing the electroplating of the other. Moreover, the user can control the chemical composition of the deposited feature through the bias tuning. See Figure 3-4 and Figure 3-5 for the two possible cases in double metal printing. The first figure for two metal ions with the same polarity and the second figure for two metals with different polarity, i.e. one cation and one anion. The metals that appear in the figures are the ones that have been used in this project.

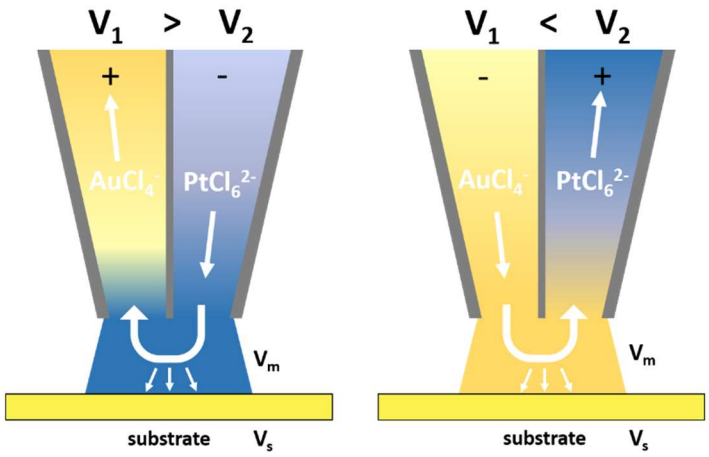

Figure 3-4. *Representation of the Au-Pt printing method using double barrel nanopipette. Effect of the bias for metal segregation when electroplating two metals with same ionic polarity.*

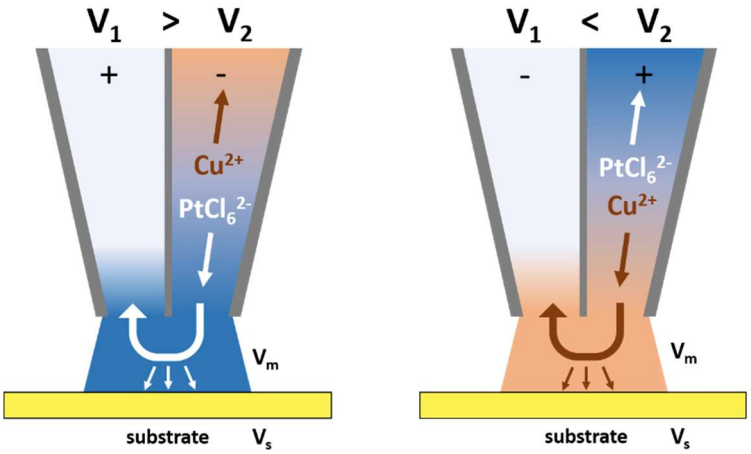

Figure 3-5. *Representation of Cu-Pt printing method using double barrel nanopipette. Effect of the bias for metal segregation when electroplating two metals with different polarity.*

On the one hand, when both metals have the same polarity (Au-Pt), they need to be contained by different barrels in order to induce the printing of one while blocking the other. When Au ions are pulled away the substrate, Pt ions are pushed towards it as both are attracted and repelled by the same electrodes simultaneously. On the other hand, when the metals have different polarity (Cu-Pt), they need to be contained in the same barrel. In this situation, when Cu ions are pulled away from the substrate, Pt ions are pushed towards it as they are attracted and repelled by the opposite electrodes.

Figure 3-4 and Figure 3-5 describe the two studied systems in this project. However, both arrangements can be extrapolated to print any pair of metals. Depending on its ion polarity, one system or the other can be implemented. The bias performance was tested and the results can be found in section 5.2.1.

An important aspect to take into account is that each metal is deposited at a different substrate voltage. Cyclic voltammetries (CVs) have been used to determine the voltages for the deposition of each metal (see 3.2.3). The substrate voltage needs to be changed at the same time that the bias changes in order to obtain the correct deposition of the desired metal.

3.2.3. Cyclic Voltammetry and Reduction Potential

Cyclic Voltammetry (CV) is an electrochemical technique which measures the current that develops in an electrochemical cell under conditions in which the working electrode potential is ramped linearly versus time. When the set potential is reached during the CV, the working electrode potential is ramped in the opposite direction to return to the initial

potential in order to close the cycle. Usually the closed cycle is repeated as many times as needed. Afterwards, the current at the working electrode is plotted versus the potential, also applied at the working electrode. This potentiodynamic electrochemical measurement is generally used to study the electrochemical properties of an analyte in solution [72, 73, 74, 75]. In the present project it is used to study the electrochemical properties of the electrolytes that contain the metal ions to be deposited.

All along this thesis, CVs have been used to detect the correct reduction potential for each metal. They have been realized employing the same printing setup, in single barrel pipettes and also in double barrel. In both cases, the working electrode is the substrate but the potential is controlled, in the first case by only one reference electrode and, in the second case, by two reference electrodes. Therefore, a scan rate has been set in the reference electrodes and a constant meniscus is maintained during the scanning. Using CVs, the reduction and oxidation potentials of the species to be printed were found for the specific setup. This project mainly focused on finding the correct reduction potential for the printed metal ions (Cu, Pt and Au).

In Figure 3-6, an example of a CV of three cycles done to an electrolyte containing $CuSO_4$ and H_2SO_4 through a single barrel pipette is shown. The figure uses the IUPAC convention [73].

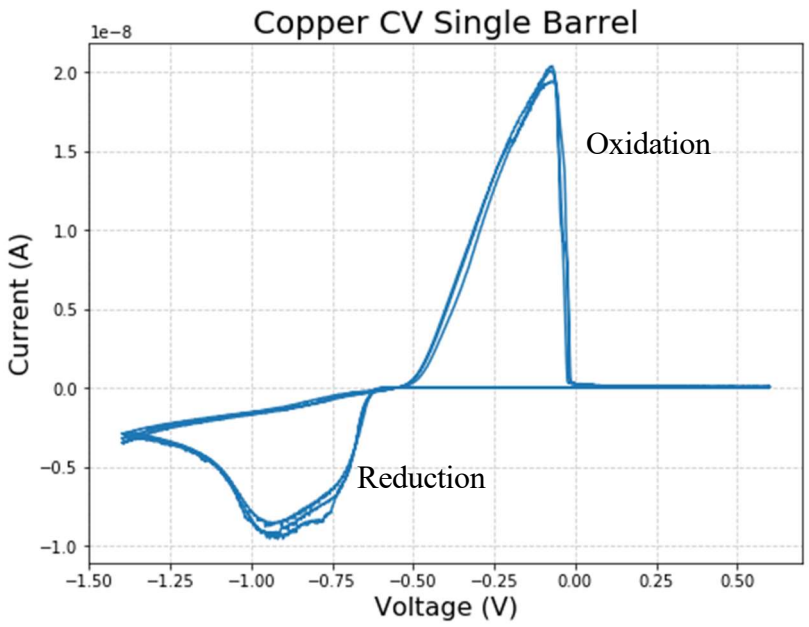

Figure 3-6. *CV of 5mM $CuSO_4$ with 1mM H_2SO_4 using a scan rate of 100mV/s, a Pt reference electrode and a Au working electrode.*

The oxidation and the reduction peaks can be found around the -0.1V and -0.90/-0.95V respectively. Therefore it is interesting to use -0.90/-0.95V or slightly higher potential in the working electrode for fast electroplating of copper. The negative currents are caused by the metal reduction while the positive come from its oxidation. The concentration of the electrolyte should not change the location of the peak, however, it might change the peak intensity. The hydrogen evolution (HE) is an important aspect to take into account when selecting the cathode reduction voltage (see 3.2.5). In the minimum cathode voltage (around -1.4V), the start of the HE can be seen as the currents start to slightly decrease again. In Figure 3-7 a deeper view of the CV of Figure 3-6 can be found.

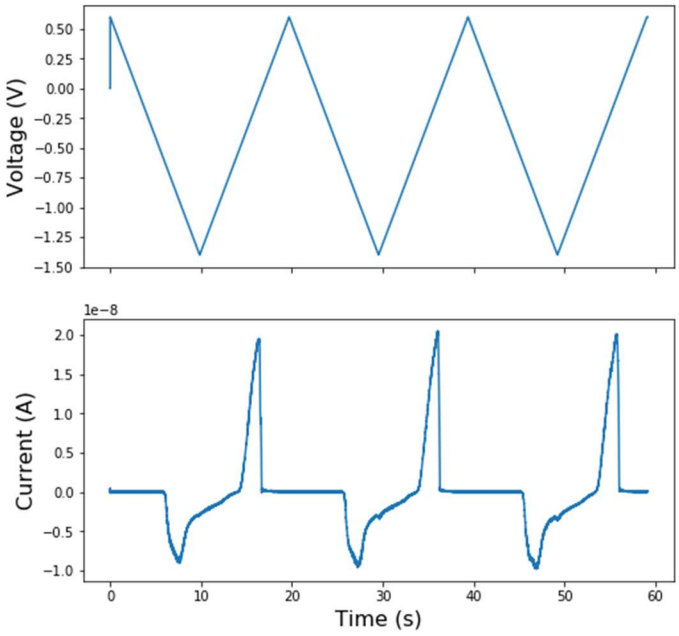

Figure 3-7. *Open representation of a CV of 5mM $CuSO_4$ with 1mM H_2SO_4 using a scan rate of 100V/s, a Pt reference electrode and a Au working electrode.*

3.2.4. Barrel Conductivity

Conductivity in each barrel has been found to be an important characteristic for the correct operation of the multi-metal printing. A good knowledge of barrel's conductivities is needed to print with double barrel.

3.2.4.1. Conductivity definition

Electrical conductivity is the property of a material that quantifies its ability to conduct electric current. In the case of study, the conductivity of the barrels depend ideally on the electrolytes contained as their ions are responsible of the charge movement when a potential drop is applied.

The ionic current density [$A \cdot m^{-1}$] can be calculated using

$$\overrightarrow{J_\rho} = -K_T \cdot \nabla\emptyset \tag{7}$$

Where K_T is the conductivity [$S \cdot m^{-1}$] and $\nabla\emptyset$ [V] is a potential drop. It exists a linear superposition of the conductivities of the different ions that each barrel contain as all of them intervene in the charge movement.

$$K_T = k_1 + k_2 + \ldots + k_N \tag{8}$$

Charged species can move through a media using two driving forces: a concentration gradient or an externally applied electric field. Each of both forces has a physical magnitude which define the degree of ease with which ions pass through the media. The diffusivity (D_i) is related to the external applied field and the mobility (u_i) is related to the concentration gradient [76]. It exists a relationship between them and it can be shown that are the same physical entity [77].

The diffusivity [$m^2 \cdot s^{-1}$] of an ion in liquid can be obtained from the Einstein-Stokes relation [78]

$$D_i = \frac{k_B \cdot T}{6 \cdot \pi \cdot \mu \cdot R_0} \tag{9}$$

Where k_B is the Boltzmann constant, T is the temperature, μ is the viscosity of the liquid and R_0 is the radius of the particle/ion. The relationship between mobility and diffusivity of an ion can be derived considering the drift velocity of ions in terms of mobility under both driving forces: an electric field and a concentration gradient [76]. Then the Nernst-Planck equation

$$D_{i0} = u_i \cdot R \cdot T; \qquad D_i = \frac{D_{i0}}{N_A} = \frac{u_i \cdot R \cdot T}{N_A} = u_i \cdot k_B \cdot T \tag{10}$$

Implies that mobility and diffusivity are interchangeable. Therefore, if we take into account the ion's charge ($F \cdot z_i$) to compute ionic conductivity, the electrolytic mobility of the ions can be defined as

$$u_i = \frac{F \cdot z_i \cdot D_i}{k_B \cdot N_A \cdot T} = \frac{q_i}{R \cdot T} \cdot D_i \tag{11}$$

Finally, the ionic conductivity derives from the ion mobility [$m^2 \cdot V^{-1} \cdot s^{-1}$] with the next equation

$$k_i = F \cdot z_i \cdot u_i \cdot c_i = q_i \cdot u_i \cdot c_i \tag{12}$$

Therefore, a relation between diffusivity and ionic conductivity can also be obtained combining equation (11) and equation (12)

$$k_i = \frac{(F \cdot z_i)^2 \cdot c_i \cdot D_i}{k_B \cdot N_A \cdot T} = \frac{{q_i}^2 \cdot c_i}{R \cdot T} \cdot D_i \tag{13}$$

3.2.4.2. Conductivity in Double Barrel

In order to be able to print correctly, barrel's conductivity has to accomplish two characteristics: to be conductive enough to ease charge movement, and to have similar conductivities in each barrel. Otherwise, the voltage obtained in the meniscus or in the substrate is not the correct that enables printing or that permits to control which barrel is printing. If the barrels have different conductivity, the barrel with higher conductivity takes control over the other in the potential generated in the meniscus. Because of this, a weight factor related to barrel's conductivities needs to be added in the formula to compute the potential in the meniscus. These weights are complex to compute and might demand for huge or small voltages that may not be ideal for the setup or the electrolytes.

$$V_m = \frac{V_1 \cdot w_1(k_1) + V_2 \cdot w_2(k_2)}{2} \tag{14}$$

Where V_1 and V_2 are the voltages applied to each barrel and $w_1(k_1)$ and $w_2(k_2)$ are the weights that depend on the respective conductivities. When both conductivities are the same, the meniscus potential accomplishes that both weights are equal to 1. Therefore

$$V_m = \frac{V_1 + V_2}{2} \tag{15}$$

A finite elements COMSOL Multiphysics model was developed to test and prove the conductivity concepts. The results can be found in section 5.2.2.

3.2.5. Hydrogen evolution reaction

Hydrogen evolution (HE) reaction is the process of generating molecular hydrogen gas (H_2) by a chemical reaction, usually from acid electrolyte in aqueous solution. Hydrogen evolves from the reaction

$$2H^+_{(aq)} + 2e^- \rightarrow H_{2\,(g)} \tag{16}$$

The whole process of HE reaction can be divided into two steps: absorption and desorption. Initially, the protons from the solution are attached to the catalytic sites of the electrode (in MCED system it is the substrate or the printed structure). Then, the electrons from the electrode combine with the protons to form hydrogen atoms. Two hydrogen atoms bond together to become a hydrogen molecule. Afterwards, desorption takes place and molecular hydrogen in gas state leaves the site of the electrode generating bubbles [79].

The hydrogen bubbles have to be avoided during the printing process. When the deposition potential is above the HE potential, the hydrogen bubble formation can agitate or break the meniscus and prevent stable deposition of metal wires. This results in a highly porous wire structure [80] instead of a solid and smooth pillar structure when HE is not taking place see Figure 3-8. There are two ways to avoid the HE in MCED printing: reducing the printing potential to not surpass the HE potential or to reduce the acidity of the electrolyte, therefore to reduce the amount of protons (H^+) in it.

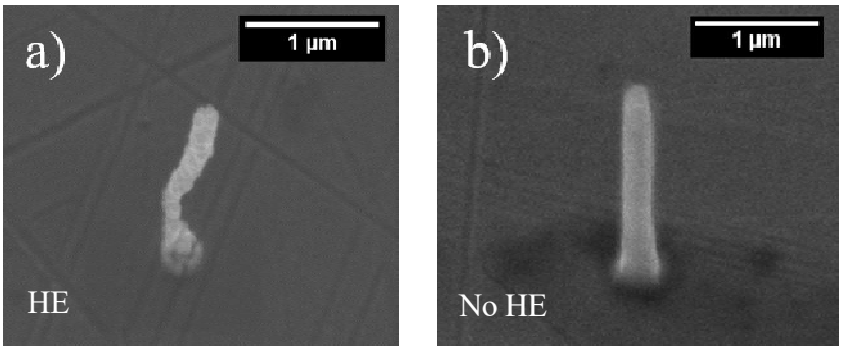

Figure 3-8. *Two Pt pillars printed with double barrel in combination with Cu (Cu-Pt system). a) 30° tilted SEM image of Pt pillar with HE. Irregular growing b) 45° tilted SEM image of Pt pillar without HE. Smooth growing.*

Two material characteristics enhance HE [81, 82]: material intrinsic activity (i.e. higher exchange current density) and large surface area. The second characteristic is less important in the MCED setup as the substrate and the structures are supposed to be similar independently of the metal being deposited. However, the actual material that is being deposited can influence the hydrogen bubbles generation. The best materials for HE are noble metals in the platinum group: Pt, Rh or Ru. Followed by transition metals: Au, Ni, Co, Fe, Cu [83]. The three metals deposited in the project can be found in these two high hydrogen catalytic groups. However, platinum is the most active one of all.

3.2.6. Electrolyte's concentration

The concentrations in the electrolytes are a key parameter for a good electroplating. The concentrations have to be high enough to ensure easy electrodeposition but not too much that might induce to pipette clogging. In addition, when using an inert salt to ensure barrels' conductivity, the user should employ the lower concentration possible in order to avoid salt crystallization in the meniscus because of electrolyte evaporation. In this project, the ideal concentrations have been found through the following process. Firstly, an initial value was chosen through literature reading, then after some experimentation this value was refined to the user setup and, finally, it was adapted to the system to match conductivities and relative concentrations between electrolytes and to minimize HE. At the end, some last testing was still done after the adaptations.

3.2.6.1. Equilibrium potential in meniscus

An effect that might appear due to the different concentrations in each barrel is the equilibrium/resting potential for membranes. This might cause some problems in the voltage adjustments if the meniscus is working as a membrane.

If the meniscus is considered as a membrane, an equilibrium potential should appear between the two barrels as each barrel contains a different concentration in the electrolyte. The ions diffuse to the opposite barrel until a membrane potential, which can balance the difference in concentration of ions between barrels, is generated. This membrane potential between the two barrels affects the bias control of the setup. If one barrel has a concentration of a metal ion but the other has none of it, a completely unknown equilibrium potential will be generated (see Figure 3-9). Approximating this potential with the Nernst equation can be found that it can reach high levels.

$$V_{eq} = \frac{R \cdot T}{z \cdot F} \cdot ln \frac{[M^+]_{barrel\ 1}}{[M^+]_{barrel\ 2}} \tag{17}$$

Moreover, this equilibrium potential will be continuously changing because as soon as the meniscus approaches to the substrate and we deposit some metal ions and we push/pull them with the bias, the concentration in the barrels will change. Therefore, this equilibrium voltage had to be fixed at a low level. In order to do so, the electrolyte of each barrel contains a dilution of one thousand of the electrolyte of the opposite barrel. With the dilution, the voltage potential is fixed during the whole printing at a relatively low level with respect to the bias and the electroplating voltages used.

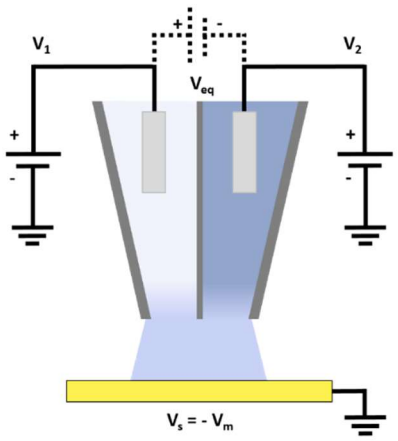

Figure 3-9. *Schematic draw of the double barrel system with the equilibrium potential due to the meniscus "membrane".*

4. Multi-Metal Meniscus-Confined Electroplating System

We already know the parameters that rule the multi-metal MCED technique at internal level. In this chapter the whole MCED setup used during this project and the way it works is presented.

4.1. System Description

A computer controlled system has been built to accomplish the multi-metal MCED. The system consists of a field-programmable gate array (FPGA) based data acquisition board, a micro- and nanomotion control, a feedback system and a visualization system. A schematic showing can be seen in Figure 4-1.

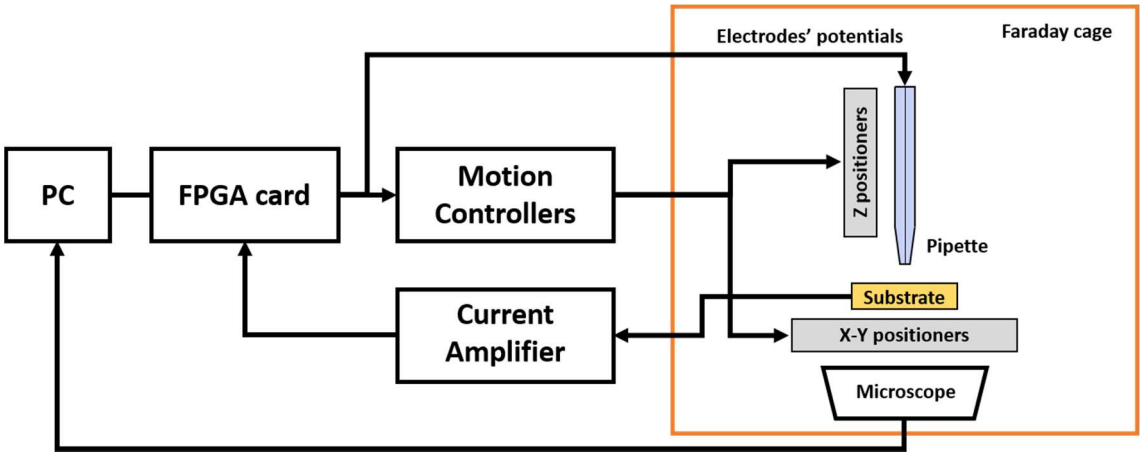

Figure 4-1. *Schematic box diagram of the general setup for multi-metal MCED.*

The FPGA card enabled fast data acquisition and control of the probe positon and potentials through embedded instructions. A PC based data acquisition system generally operates at 10-20KHz, where the FPGA card used can perform at 500MHz. In the schematic box diagram two ways of observing the printing process in real time are found: the visual through the microscope utilized by the user and the ionic current measurements used by the control program.

In Figure 4-2 two pictures of the experimental setup built for printing multi-metal nanostructures can be found.

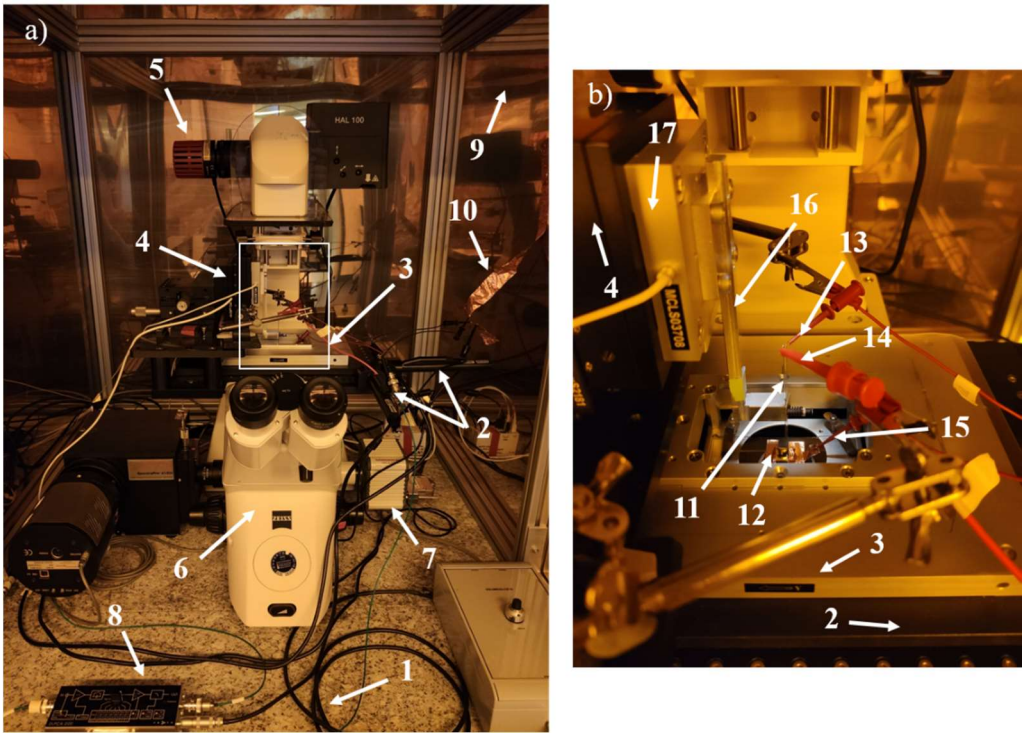

Figure 4-2. *a) Experimental setup for multi-metal MCED. b) Magnified image for the area marked with a white square in Figure 4-2a. The labels in the figure represent: (1) anti-vibrations air table, (2) coarse X-Y stage actuators, (3) fine X-Y nanopositioner stage, (4) coarse Z stage, (5) LED light, (6) inverted microscope, (7) digital camera, (8) current amplifier, (9) Faraday cage, (10) common grounding, (11) nanopipette, (12) substrate and sample, (13) electrode V_1, (14) electrode V_2, (15) connection to substrate cathode, (16) pipette holder, (17) Z nanopositioner.*

4.2. Motion Control

The setup was placed on an optical table to reduce the effect of vibration-induced disturbances during the electrodeposition process. The motion control was divided into two systems: the horizontal X-Y system and vertical Z system. Each axis was comprised by a coarse-positioner actuator and a precise piezoelectric nanopositioner. On top of the coarse movement horizontal stage, a two axis X-Y high speed piezoceramic nanopositioner stage was mounted to provide an ultra-fine positioning. For the movement along Z axis, a programmable micropositioner motor was employed. Emplaced to the Z stage, a compatible high speed piezo nanopositioner was used for the fast, fine and precise vertical positioning. All the stages were connected through their own controllers to a single computer and a FPGA. The whole setup was controlled by a set of LabVIEW programs.

4.3. Current Measurements

The measurements of the current signals play a crucial role in the electrodeposition growth in the multi-metal MCED setup as they are used as feedback signal while printing. The printing method is based on a repetitive approach and retraction of the pipette to the substrate in order to form and destruct the meniscus constantly. When the pipette is in the air, the electrolytic cell is no formed and an open circuit is created, therefore, there is no current flow. But once the meniscus is formed between the pipette tip and the substrate, electrodeposition starts taking place. This triggers the appearance of a faradic current signal. As soon as the faradic current surpasses an imposed threshold, the pipette is retracted to prevent clogging. Then the meniscus is broken and the cycle starts again when the pipette approaches the substrate to create a meniscus again.

The electrical noise level of the amplifier sets the lower limit of the possible threshold. Therefore, the optimal noise configuration of the Lock-in amplifier was employed. The base signal (open circuit) had an offset of around -6pA and a standard deviation of 5pA approximately. With this configuration the amplifier provided a rise time (defined as the time for the current to change from 10% to 90% of the maximum current signal) of 7µs.

In most of the experiments, a threshold between 10pA and 100pA was employed. This threshold allowed depositions of metal disks of several tenths of nm per approach. In order to reduce the noise, the setup was build inside a grounded Faraday cage.

4.4. Experiment workflow

4.4.1. Pre-printing process

A traditional MCED 3D printing starts with the pipette fabrication and preparing the electrolytes that will act as ions reservoirs to be deposited. Two different electrolytes are needed, one for each barrel. The double barrel pipette is filled with the electrolytes using a micro-filler. The barrels need to be marked to be able to differentiate between them and, then, the pipette has to be kept in nozzle-down position for few minutes, such that the solution reaches the very tip of the nozzle because of the capillary forces and all the internal air bubbles rise up to the outside. This last step becomes more critical as the pipette aperture gets smaller.

While waiting for the capillary forces to do their job, the substrate is placed on top of the stage and connected to the current amplifier. Next, using the coarse X-Y stage movement, the printing position can be stablished. Once the nanopipette is ready, it is mounted into the

probe holder. It consists on a metal part with a groove and a metal sheet that holds the pipette into the groove through the force applied by a spring. At this point, the barrel electrodes are introduced in the respective barrels and connected to the correspondent power supplies. Then, a coarse movement along Z axis is carried out with the micropositioner to bring the nozzle closer to the substrate. This movement is monitored with a microscope. When the pipette is close enough to the substrate (around 100µm), the electric noise is checked and afterwards, a LabVIEW program is launched for precise approach.

This program performs a synchronous movement of the micro- and nanopositioner. The nano stage moves 30µm (nanopositioner working range) at 3µm/s towards the substrate to detect it. If the substrate is not detected, the nanopositioner retracts completely to its initial state and the micropositioner approaches 25µm. Then, the cycle is repeated in a loop until the pipette lands on the surface. As soon as the meniscus is formed, the electric circuit is closed and a current peak is observed. Once the pipette lands, the nanopositioner does a last retraction. At this point, the substrate is detected and, furthermore, the distance between the nanopipette and the substrate falls in the working range of the nanopositioner. The LabVIEW program is terminated and the setup is ready to start printing.

4.4.2. Printing process

In order to obtain high-quality nano-structures with the MCED technique, a precise responsive control of the probe-to-substrate positioning and a fine control of material delivery is required.

After having detected the substrate position and having the probe within the nanopositioner working range, the printing process is ready to be started. The printing process is carried out through a LabVIEW VI with a .csv (comma separated value) document as input. Each .csv row incorporates X and Y position of the voxels, the type of feedback used, the height Z of the voxel, the voltage in the electrodes V_1 and V_2, the update position time, the feedback threshold and finally the retract speed factor. Table 4-1 provides a description of all the parameters involved in the process of printing.

As soon as the .csv file is uploaded, the printing process begins. The .csv is read row by row and each row defines a voxel. Usually the first voxel of the printing session has a different feedback type with respect to the others. In the first voxel, the exact position of the substrate is defined and this information is used when printing all the other voxels to avoid mismatching between pillars.

Parameters	Description
Feedback threshold	Set point, when overshooted by DC current indicates meniscus formation
Feedback type	Type of feedback used when printing the voxel.
Approach velocity	Initial approach speed of the probe for the first positioning
Retract speed	Speed of the probe when it retracts from the surface
Retract distance	Distance to retract after hitting the set point
Voxel height	Defines the height of the voxels
X position	X coordinates of the voxel to be printed
Y position	Y coordinates of the voxel to be printed
V_1 voltage	Voltage in electrode of barrel 1
V_2 voltage	Voltage in electrode of barrel 2
Lateral scan rate	Speed of the probe when it moves laterally to one coordinate to the next
Hopping approach rate	Speed of the probe when approaches the surface once it is on the new printing coordinate
Hopping retract rate	Retraction speed of the probe on completion of a voxel
Update position time	Time between probe position updates
Upper limit of dz	Single step length of Z positioner
Retract speed factor	Incremental factor for the Z nanopositioner movement

Table 4-1. *Parameters defined in printing VI. The bold parameters can be changed for each printing voxel, the non-bold are global parameters for the whole print.*

The probe moves towards the surface and when the liquid meniscus interface is created electrodeposition takes place and it continues until feedback threshold is reached. The approach of the pipette is defined by piezo approach rate (1 in Figure 4-3).

$$piezo\ approach\ rate = \frac{(dz\ limit) \cdot (piezo\ resolution)}{update\ position\ time} \tag{18}$$

Upon reaching the current threshold, the probe is retracted with a retract speed (2 in Figure 4-3)

$$piezo\ retract\ rate = \frac{(dz\ limit) \cdot (retract\ speed\ factor) \cdot (piezo\ resolution)}{update\ position\ time} \tag{19}$$

The growth of the voxel continues layer-by-layer (h_1 and h_2 in Figure 4-3 represent the layers height growth) until the desired voxel height is achieved. Once the voxel is finished, the

probe is retracted with hopping retract rate (3 in Figure 4-3) and moves towards the next voxel coordinates with lateral scan rate (4 in Figure 4-3) followed by an approach for starting the growth of the next voxel with a hopping approach rate (5 in Figure 4-3).

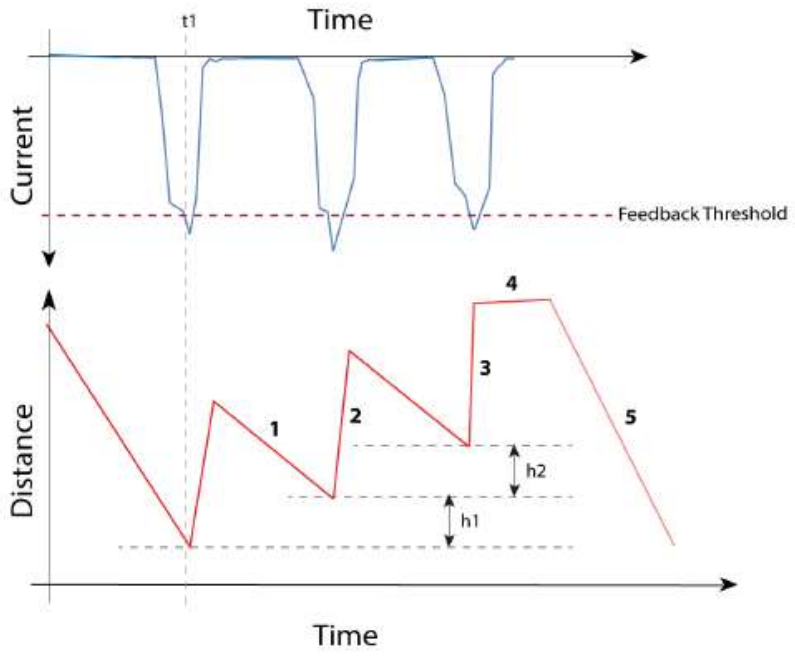

Figure 4-3. *Simplified example of the current and vertical displacement evolution when printing a voxel.*

In Figure 4-4 the z-Position, the electrodes' voltages and the electrodeposition currents of the printing process of a two metal wire (Au-Pt) are shown. Every approach and retract of the probe and the continuous growth of the pillar can be observed in the z-Position graph. The central spike with the longest retraction takes place when the metal deposited changes. At the current graph, the spike of each approach when the meniscus is formed and electrodeposition initiates can be observed (when depositing the current is positive because of the reference). Also that the deposition current of one metal is slightly higher than the other. Finally, the voltages of the two electrodes can be observed. To change the metal that is being deposited they have to change.

From the printing data, the deposition speed and the radius of the pillar can be computed. Usually the deposition speed is obtained through

$$Deposition\ speed = \frac{pillar\ height}{printing\ time} \tag{20}$$

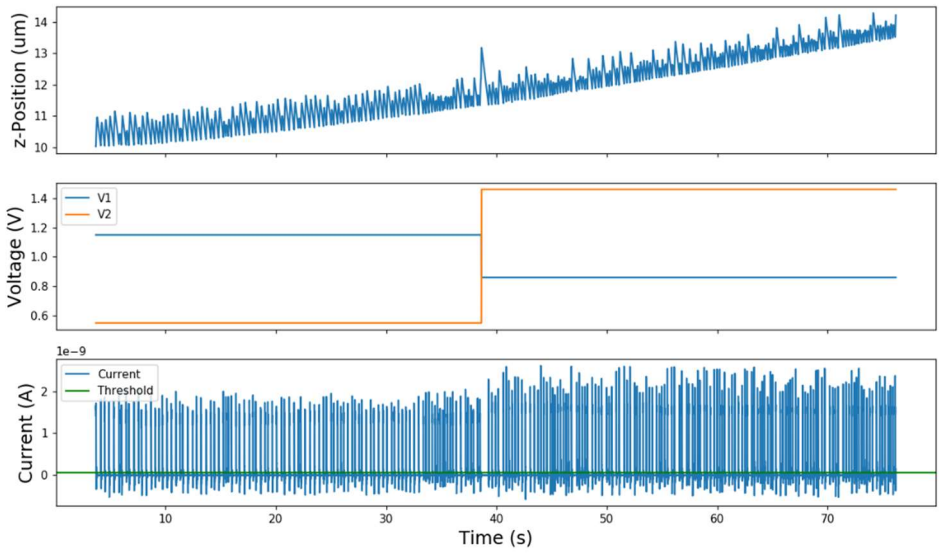

Figure 4-4. *Data obtained from printing a Au-Pt pillar of 3.6μm tall.*

To compute the radius of the pillar, the Faraday's law of electrolysis is used. The mass of metal (m) elements deposited at an electrode is directly proportional to the charge (Q) in Coulombs. The law can be expressed as

$$m = \frac{M}{n \cdot F} \cdot Q \tag{21}$$

where M is the molar mass of the deposited metal, n is the number of electrons transferred by the ion into solution and F is the Faraday's constant.

The amount of electric charge Q can be calculated by integrating the current over the duration of each spike (see Figure 4-3 and Figure 4-4). If we take into account the volume V of the metal deposited instead of the mass m using the material density D

$$V = \frac{M}{n \cdot F \cdot D} \cdot Q \tag{22}$$

Then the radius can be calculated if the deposited metal for each current spike is approximated by a disk. The height of the deposited disk is known through the reading of the vertical displacement of the piezo positioner ($h = \Delta z$ between approaches). Therefore, if

the volume of the deposited disk is $V = \pi \cdot r^2 \cdot h$, the radius of the pillar can be approximated using

$$r = \left(\frac{M \cdot Q}{\pi \cdot n \cdot F \cdot D \cdot h}\right)^{1/2} \tag{23}$$

An average of the radius along the pillar is calculated because, usually, the first approaches towards the substrate generate a wider meniscus as it has a lot of surface to extend on. As soon as the initial disks are deposited, the meniscus is no longer formed on the substrate but on the already deposited disks. Then, the meniscus stabilizes after several approaches.

To finish this chapter, an image of the usual visualization of the printing area offered by the setup is presented. The round dark dots in matrix order are the pillars that have been printed. The dark area in the left of the image is part of a cross done with a marker to locate the structures.

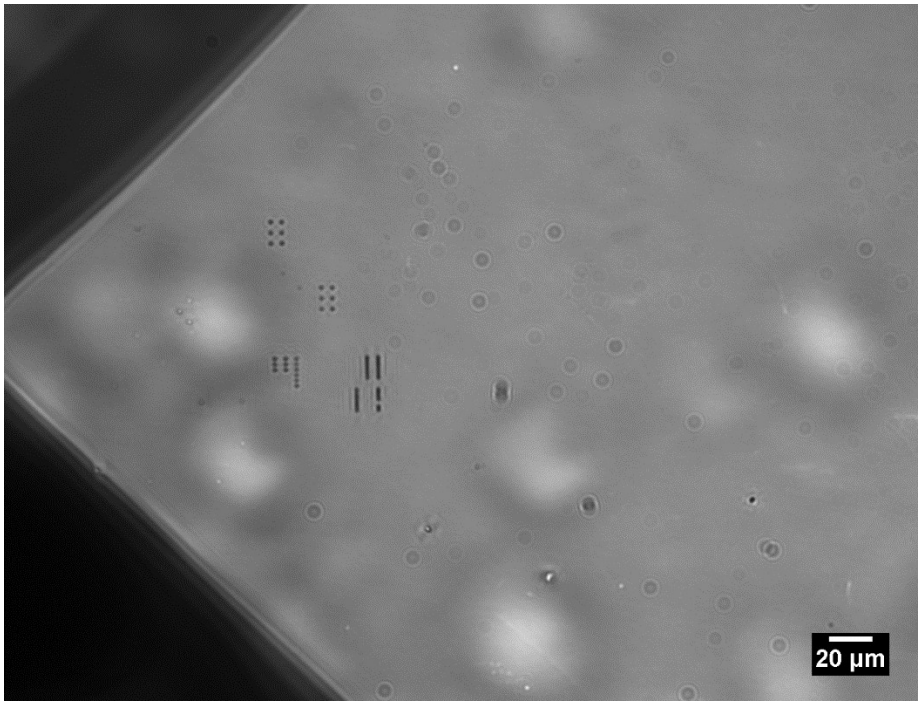

Figure 4-5. *Printing area visualization through the inverted microscope with a x20 magnification lens.*

5. Results and Discussion

In this section the main experimental results of the project are reported. Simultaneously, we discuss their interpretation and describe advantages and limitations of the proposed solutions and developed techniques. First, the results of printing a new metal with single barrel are presented. Second, the bias performing and the importance of the conductivities in each barrel are tested. Thirdly, the characterization of the multi-metal printed structures is done. Finally, the results of the structures releasing attempts are exposed.

5.1. Printing a new metal

The goal of the project was to develop a method for multi-metal printing with the MCED system. In order to advance towards this goal, we first needed to characterize and control the printing of the individual metals that we were going to combine in the multi-metal system. In this first results chapter, the electroplating characterization for the single barrel MCED of the three studied metals (Cu, Pt and Au) is going to be presented.

5.1.1. Printing Copper

Copper (Cu) is a soft, malleable, and ductile metal with very high thermal and electrical conductivity. It has been used for printing circuit boards as well as for electrical connections in integrated circuit chips during decades. The most used electrolyte for copper electroplating is $CuSO_4$ in aqua solution. Some sulfuric acid was added to ensure a good dissolution of the metal and an acidic medium for printing. The $CuSO_4$ electrolyte is obtained from the solution of copper (II) sulfate pentahydrate. The basic electrochemical reaction of this copper electrolyte is

$$Cu^{2+}_{solution} + 2e^- \rightarrow Cu_{lattice} \tag{24}$$

The copper cation gets reduced and deposits in the cathode in an ordered lattice structure. Copper is the metal more used in MCED literature for its easy electrodeposition, its good electric properties, and a cathode reduction potential far from HE. A CV analysis of the copper electrolyte can be found in Figure 3-6 using Pt and Au electrodes. The cathodic reduction and oxidation peaks are found at a substrate voltage of -0.92V and -0.1V, respectively.

5.1.2. Printing Platinum

Platinum (Pt) is a dense, malleable, ductile, highly unreactive metal. It is highly resistant to corrosion and it is considered a noble metal. Platinum is used in catalytic converters, laboratory equipment, electrical contacts and electrodes and also for medical implants. For electrodeposition of patinum, chloroplatinic acid (H_2PtCl_6) is used. This acid is obtained through the dissolution of platinum in hot aqua regia [84].

$$Pt + 4\,HNO_3 + 6HCl \rightarrow H_2PtCl_6 + 4\,NO_2 + 4\,H_2O \tag{25}$$

When the chloroplatinic acid is used as printing electrolyte, a two-step irreversible reduction takes place [85, 86].

$$[PtCl_6]^{2-} + 2e^- \rightarrow [PtCl_4]^{2-} + 2Cl^- \tag{26}$$

Initially, $[PtCl_6]^{2-}$ ion reduces to $[PtCl_4]^{2-}$ by gaining two electrons from the cathode, which further reduces to $Pt(0)$ metal by the following reaction.

$$[PtCl_4]^{2-} + 2e^- \rightarrow Pt(0) + 4Cl^- \tag{27}$$

Printing in a weakly acidic solution (pH > 2) contribute to the electrodeposition of Pt [87]. Platinum is a good catalyst for HE and it can be seen in its CV as the hydrogen generation starts at a higher cathode potential. In Figure 5-1 the CV of 5mM H_2PtCl_6 in aqueous solution. The peaks P_1 and P_2 indicate the two reduction reactions (26) and (27). As the potential increases further, the reduction current continues to rise due to the reduction of platinum ions but also because of hydrogen ions.

In the case of platinum, its printing voltages window is much more narrow compared to copper and gold as the HE overlaps with the reduction peak to Pt(0). A thorough refining of the printing voltage was realized. In the following figures, the study of printing speeds and feedback currents during printing is represented.

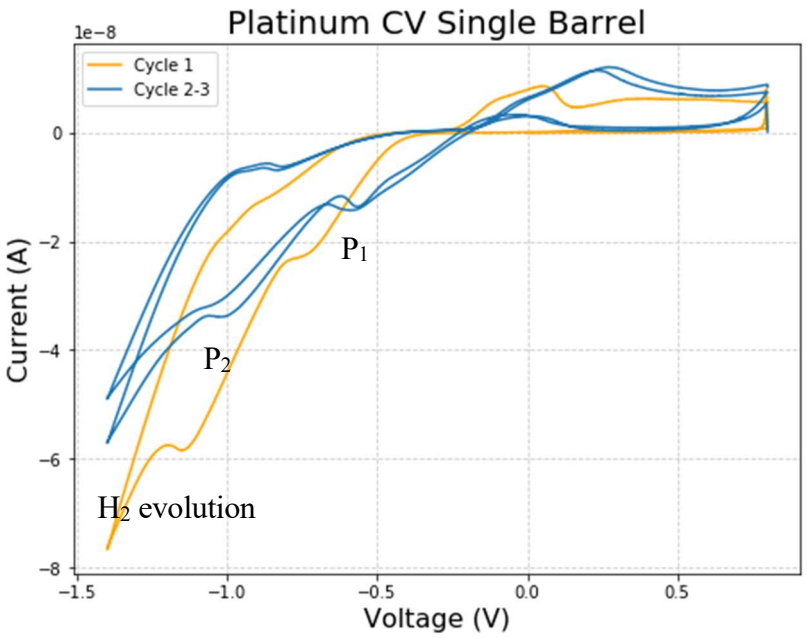

Figure 5-1. *CV of 5mM H_2PtCl_6 using a scan rate of 100mV/s, a Pt reference electrode and a Au working electrode (substrate). The orange CV is the first cycle, the blue CV are cycle 2 and 3.*

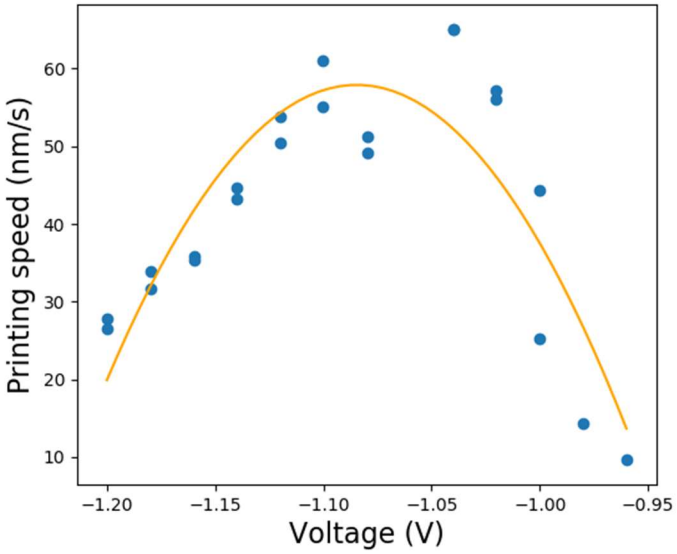

Figure 5-2. *Printing speed of 5mM Pt in single barrel vs. substrate voltage using a Pt electrode and a Au substrate. Some potentials have only one pillar data because the setup failed in printing the other. The fitting line is a second order polynomial added to highlight the tendency. It has a R^2 of 0.75.*

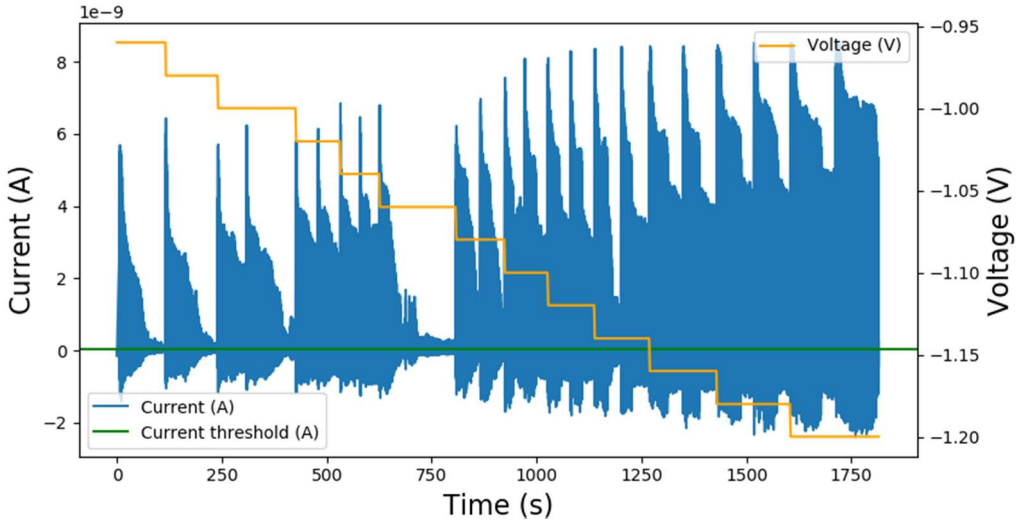

Figure 5-3. *Feedback current and substrate voltage vs. time during the 5mM Pt in single barrel speed test. The feedback current has opposite sign than the reduction current.*

From Figure 5-2 and Figure 5-3 it is found that the best printing voltage for Pt electrolyte in the used setup is around -1.08/-1.10V. At that voltage, the printing speed is maximum and the currents are stable. Comparing both figures, the effect of HE can be detected. Although the currents keep increasing while increasing the voltage (Figure 5-3), the depositing speed starts decreasing when the HE takes place (Figure 5-2). The rise of current is caused by the reduction of hydrogen. The inconsistent low current in an intermediate voltage is due to a printing error.

Finally, a SEM picture of a 4µm Pt wire printed from a 10mM H_2PtCl_6 electrolyte using the single barrel technique with -1.10V in the substrate electrode is attached.

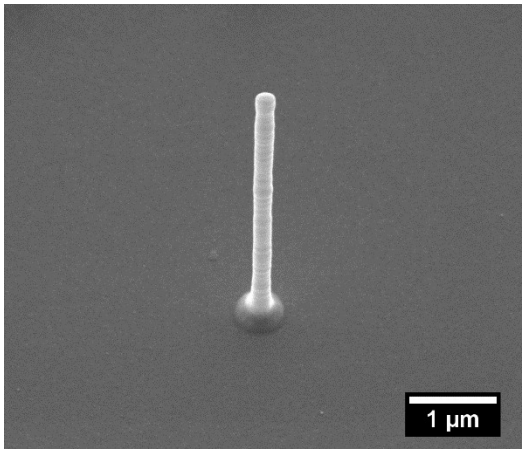

Figure 5-4. *Single barrel Pt pillar. 10mM H_2PtCl_6 electrolyte with -1.10V in the substrate. It has a height of 4µm and an average diameter of approximate 210nm.*

5.1.3. Printing Gold

Gold is also a transition metal. It is dense, soft, malleable and ductile. It is resistant to corrosion and to most acids, though it does dissolve in aqua regia which forms a tetrachloroaurate anion. As with platinum, the tetrachloroaurate anion is used for electrodeposition and it is obtained from the chloroauric acid HAuCl4. This acid is reduced following [88, 89]

$$[AuCl_4]^- + 3e^- \rightarrow \text{Au}(0) + 4Cl^- \tag{28}$$

In Figure 5-5 the CV of gold can be found. It has a clear reduction peak voltage at -0.8V and the HE starts in voltages above -1.5V. The printing window compared to platinum is broader. So it does not need such a fine voltage refining as platinum electroplating does.

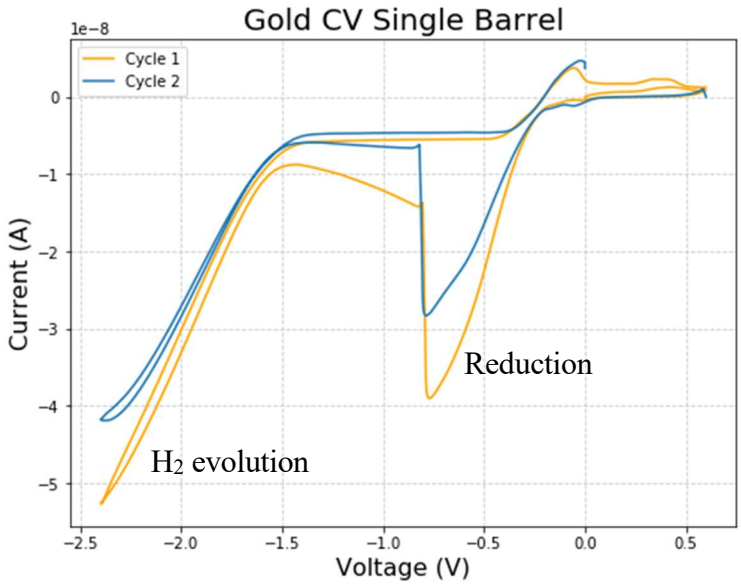

Figure 5-5. *CV of 20mM $HAuCl_4$ using a scan rate of 100mV/s, a Pt reference electrode and a Au working electrode (substrate). The orange CV is the first cycle, the blue is the second.*

Finally, a SEM picture of a 4µm Au wire printed from a 20mM $HAuCl_4$ electrolyte using the single barrel technique with -0.85V in the substrate electrode is attached.

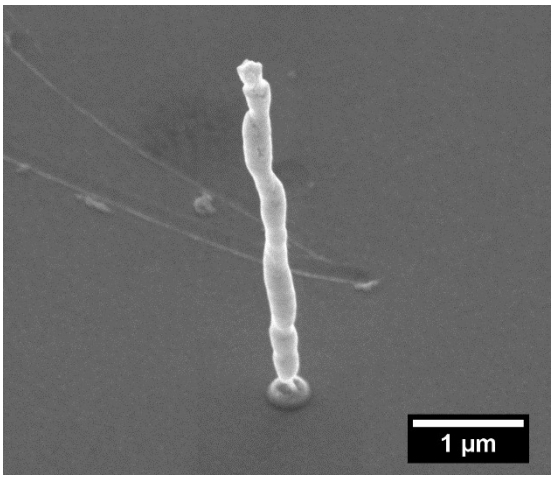

Figure 5-6. *Single barrel Au pillar. 20mM $HPtCl_4$ electrolyte with -0.85V in the substrate. It has a height of 4µm and an average diameter of approximate 230nm.*

5.2. Multi-Metal Printing

The three metals have been characterized in the single barrel setup. Now they have to be tested in the multi-metal system. However, before, we need to study the bias and confirm its well-functioning. In addition, a COMSOL model for conductivities analysis is presented.

After the results of the testing of the theoretical hypothesis of the multi-metal technique, the results of the two multi-metal printing systems defined for Cu, Pt and Au are going to be presented.

5.2.1. Study of the bias between barrels

5.2.1.1. Printing speed test

The conceptual experiment of double barrel setup with a barrel that contains an inert salt solution and the other barrel that contains a solution with the copper ions (Cu^{2+}) presented in Figure 3-3 was experimentally tested. The two barrels of a nanopipette were filled with the following electrolytes: 10 mM $CuSO_4$ and 1 mM H_2SO_4 in one barrel and 14 mM Na_2SO_4 and 1 mM H_2SO_4 in the second barrel. Then vertical pillars (same height) were printed using the electroplating voltage of copper and different biases, two for each bias. The results can be seen in the Figure 5-7 and Figure 5-8.

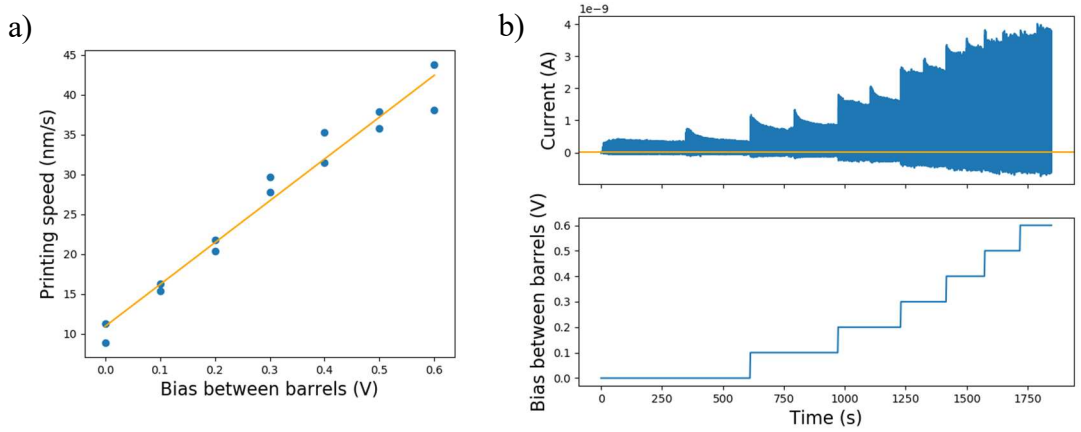

Figure 5-7. *Positive bias applied between barrels. a) Speed of Cu pillar deposition vs. the applied bias. b) Current of Cu pillar deposition vs. the applied bias and time.**

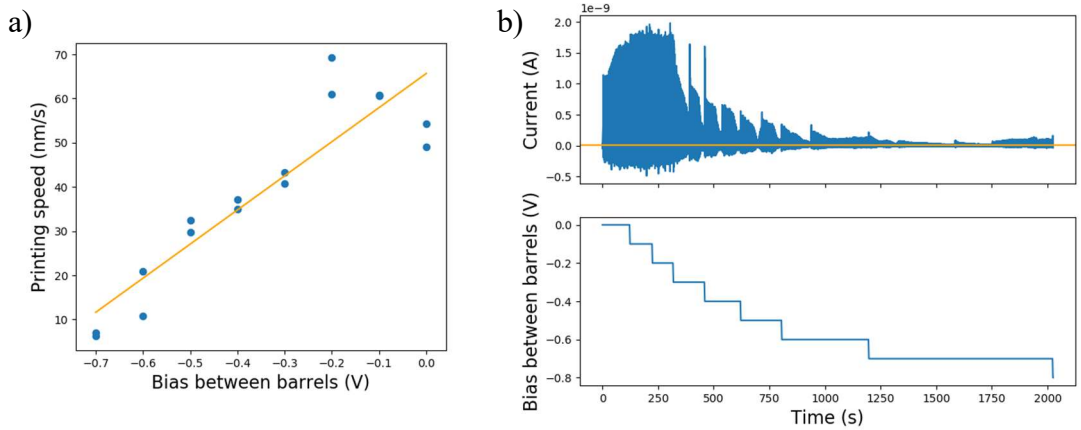

Figure 5-8. *Negative bias applied between barrels a) Speed of Cu pillar deposition vs. applied bias. b) Current of Cu pillar deposition vs. applied bias and time.**

***Note:** Both tests were realized with different pipettes. The negative bias test for the same pipette as Figure 5-7 can be found in the Appendix (page 81). The pipette used in Figure 5-8 was initially similar to the one in Figure 5-7 but a larger diameter tip was imposed in order to obtain clearer results in the effect of the negative bias because working under 10 nm/s speed is really unstable. This is why the printing speed between Figure 5-7a and Figure 5-8a in zero bias does not match.

Figure 5-7a and Figure 5-8a show the relation of the printing speed of the metal with respect to the bias applied between barrels. The printing speed is a good indicator to quantify the electrodeposition intensity. It is computed dividing the printed pillar height with the time spent in printing the pillar (equation 20). If the printing is fast, it means that a lot of metal is

being electroplated and therefore the growth is fast. Conversely, if the printing is slow, the growth is slow which means that few metal ions are electroplated in each approach. Finally, if the speed is zero, no printing is taking place. In this experiment we see how the bias has an influence on the printing speed.

In the printing speed graph of Figure 5-7 the printing becomes faster as the positive bias gets higher. The speed grows linearly to bias with a R^2 of 0.97. With a bias of 0.7V, an almost four times faster printing speed is obtained. This is because, due to the positive bias, copper ions are being pushed towards the meniscus enhancing electrodeposition. In Figure 5-8a the printing speed decreases as the bias gets smaller (more negative). It decreases also linearly to bias with a R^2 of 0.83. A negative bias of -0.7V reduces the printing speed for a factor of almost seven. The metal ions are pulled away from the meniscus diminishing the electrodeposition rate.

In Figure 5-7b and Figure 5-8b the faradic current changes with respect to time and bias. The currents are also an indicator of electrodeposition intensity. The higher current is measured, the more ions are electroplated. In parallel to the printing speed, the currents increase with the positive bias (Figure 5-7b) and they decrease with the negative bias (Figure 5-8b).

With this experiment, the effects of the bias in a double barrel nanopipette system have been shown. We can enhance or diminish electroplating through the bias tuning and any intermediate level of deposition can be obtained.

5.2.1.2. Influence of bias in cyclic voltammetry

The right operation of the bias system was also tested by developing the CVs with the multi-metal setup. The effect of the bias in CV of multi-metal setup can be observed in Figure 5-9. The CV of the next figure was done in a double barrel with 10 mM $CuSO_4$ and 1 mM H_2SO_4 in one barrel and 14 mM Na_2SO_4 and 1 mM H_2SO_4 in the second barrel. The same electrolytes of the copper bias test (Figure 5-7 and Figure 5-8) but in a different pipette with a remarkable larger aperture (around 4-8µm in diameter) were used.

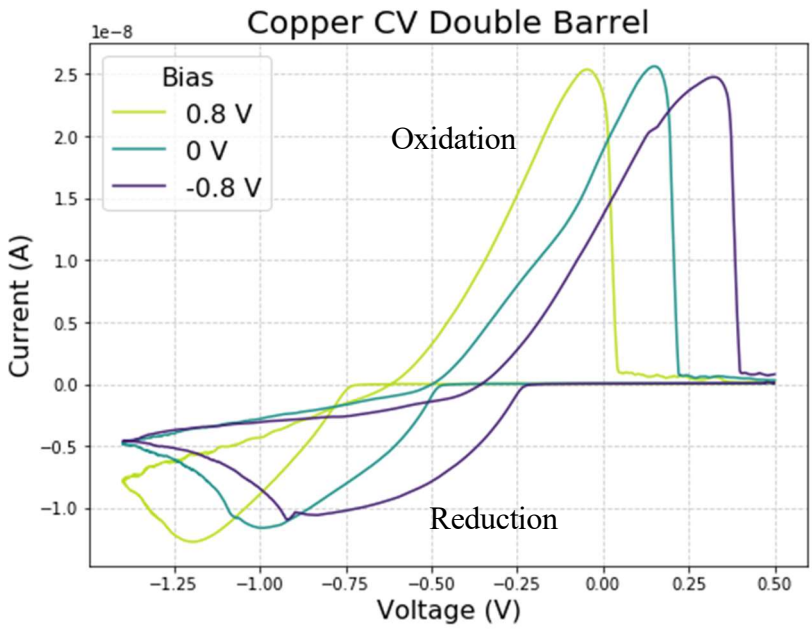

Figure 5-9. *Effect of bias in CV. Two effects are observed: the reduction peak intensity change and the reduction peak voltage shift. In this experiment, positive bias induces electroplating, negative bias reduces it.*

The peak intensity of reduction was affected by the bias. When the bias was in favor of the deposition of a specific metal, its reduction peak increased and when the bias was against the deposition of this same metal, the reduction peak decreased. The bias has another effect on the reduction of the metals, it does not only induce or prevent the reduction reaction, but it also introduces a shift in the reduction peak voltage.

The effect of the bias can be detected in the CV for double barrel. However, the reduction and increment of current is not affected proportionally as it is when the aperture of the pipette is at the nanometric level. The bias impact is proportional to the pipette aperture with a bigger impact when it is small.

5.2.2. Conductivity Simulations

A finite elements COMSOL Multiphysics model was developed to test and prove the conductivity concepts. It consists on the tip of a pipette with two barrels only connected through the meniscus formed at the tip (only half of the pipette because symmetry applies). Each barrel contains an electrolyte with a specific isotropic conductivity and a potential is applied between both barrels (see Figure 5-10). Both barrels are in contact in the meniscus and a perfect mixture is supposed, therefore, because of linearity (equation 8), its conductivity is the average between both barrels.

$$k_m = \frac{k_1 + k_2}{2} \tag{29}$$

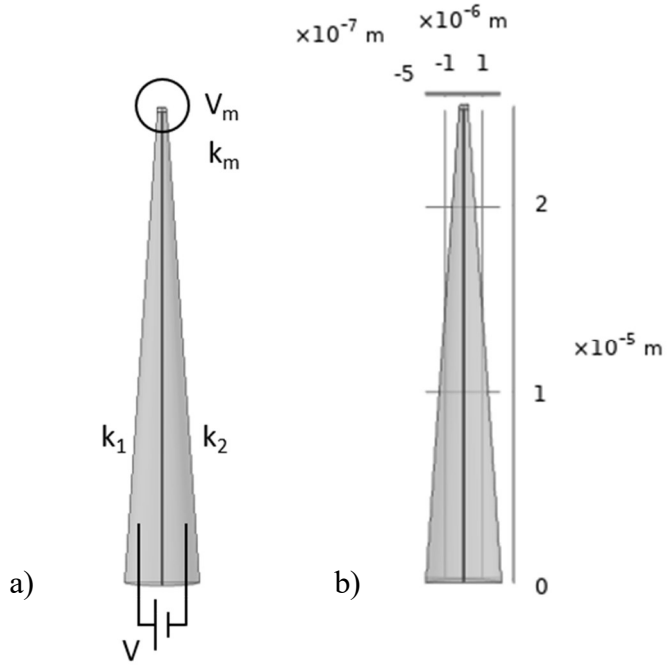

Figure 5-10. *Schematic figure of the electrolyte conductivity model.* ***a)*** *A voltage V is applied between both barrels that have specific conductivities. The conductivity k_m in the meniscus is calculated using (equation 22) and the voltage V_m is obtained through the simulation.* ***b)*** *The radius of the tip of the pipette is 250 nm, the total height is 25 um, it has 4° of aperture, a wall thickness of 50nm and the meniscus height is 250 nm*

In the next table a summary of different experiments is presented. The conductivities used were calculated analytically from the concentrations of the electrolytes employed during a laboratory test. The simulations show the effect of the conductivities in the meniscus voltage. When conductivities in both barrels are the same, the meniscus voltage is the average between barrels. When conductivities are different, the meniscus voltage is closer to the voltage in the high conductivity barrel. The importance of imposing similar conductivities in each barrel is shown through this simulation.

Experiment	Barrel	Conductivity (k) [S·m^{-1}]	Voltage (V) [V]	Meniscus Voltage (V_m) [V]
1	1	1.8	1	**0.923**
	2	0.14	0	
2	1	1.8	1	**0.5**
	2	1.8	0	
3	1	0.14	1	**0.077**
	2	1.8	0	

Table 5-1. *Influence of different conductivities in the meniscus voltage.*

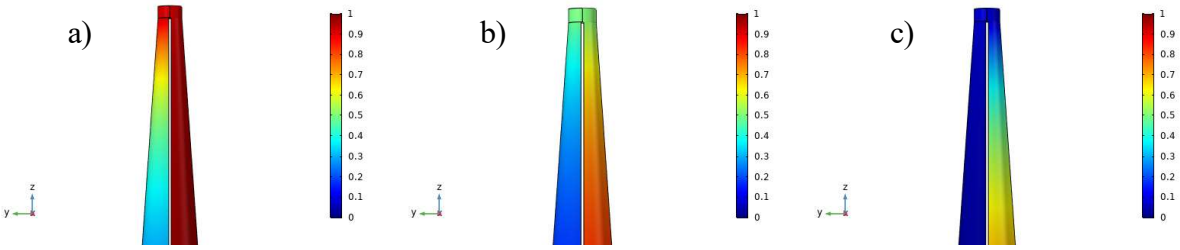

Figure 5-11. *Visualization of the voltage [V] in the tip of the pipette and in its meniscus for each experiments. The right barrel is barrel 2 and the left barrel is barrel 1. a) For experiment 1, b) for experiment 2, c) for experiment 3.*

In order to obtain the same conductivities in each barrel two main approaches were taken: to modify the concentrations of the electrolytes in each barrel (when concentrations are not critical for printing) or to add a salt that does not interact with the ink electrolytes. On the one hand, in Au-Pt system the first approach was used as the inks are in separate barrels and gold electrolyte interacts with the used salt. On the other hand, when printing Cu-Pt, the second approach was the chosen as both inks are in the same barrel and a large difference in concentrations may cause more cross-contamination when printing. The final conductivities used in each barrel for each pair of metals can be found in Table 5-3.

5.3. Multi-metal MCED printing

The expected operation of the bias and the importance of barrel's conductivities have already been demonstrated. In this chapter, the results obtained with the two multi-metal MCED

systems developed in this project are presented. Two main tests were realized to prove the right performance of the multi-metal MCED technique. The first consists in printing the two metals the most pure possible in two type of structures: pillars of a single metal intercalating between the two metals and pillars with parts of different metals, usually half-half and combining the two possible orders (1-2 and 2-1). The second consists in printing a two row array of pillars where the bias gets modified pillar to pillar. Starting for a -1V bias up to a 1V bias with steps of 0.1V. When a bias that enhances one metal deposition is being used, its reduction voltage is applied.

The results of the two tests are presented in this chapter for the two multi-metal systems developed. The images were taken with a Scanning Electron Microscope (SEM) and Energy-Dispersive X-ray Spectroscopy (EDXS) was used for the chemical characterization of the samples.

5.3.1. Copper – Platinum Multi-Metal Printing

Copper-Platinum was the first multi-metal system tested and developed. Copper had been already widely used and studied before the start of this project. Therefore, we had good knowledge about copper deposition. The first metal added was platinum because of its unique properties in the electrical field and its biocompatibility. The Cu-Pt double barrel system has been the most studied as it was the first combination used to develop the multi-metal system.

Copper is found as a divalent cation, Cu^{2+}, while platinum in solution is present in a form of anion with $PtCl_6^{2-}$. Therefore, as seen in Figure 3-5, both are located in the same barrel with a similar concentration and it contains an electrolyte with H_2PtCl_6, $CuSO_4$ and H_2SO_4. In the opposite barrel, an electrolyte with the salt Na_2SO_4 and H_2SO_4 provide an acid medium and the same conductivity than the barrel with the metal salt solutions. A lot of concentrations and voltages combinations were tested in order to find the best one. For the following figures, one barrel contained **10mM H_2PtCl_6 + 10mM $CuSO_4$ + 1mM H_2SO_4 + x1000 diluted the opposite barrel** and the other contained **70mM Na_2SO_4 + 1mM H_2SO_4 + x1000 diluted the opposite barrel**.

As seen in 5.2.1.2, the bias shifts the correct electroplating cathode voltage. Because of this, after having developed several CVs with different bias, the two potential used for Cu and Pt were -1.0V and -1.16V respectively.

5.3.1.1. Two metal pillars test results and discussions

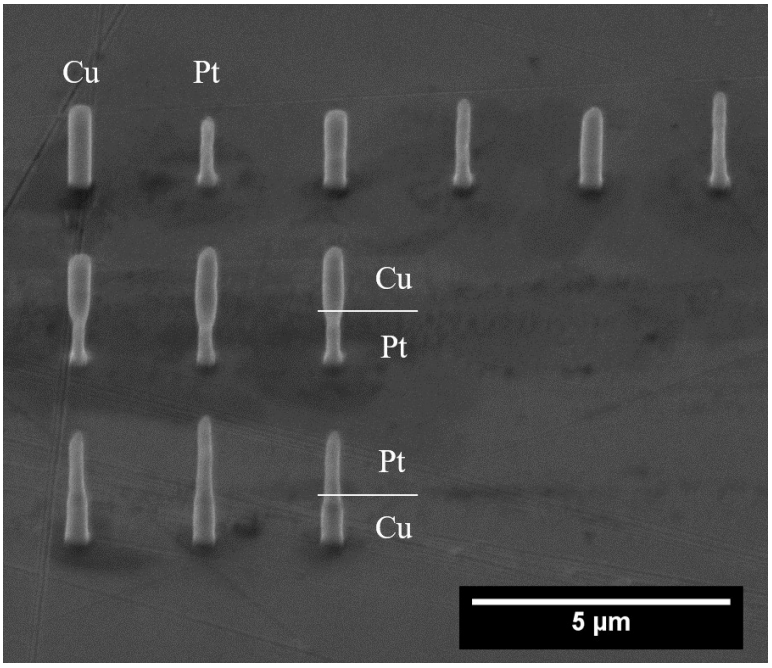

Figure 5-12. *Two metal pillars test for Cu-Pt system. Electrolytes: barrel 1) 70mM Na_2SO_4 + 1mM H_2SO_4 + x1000 diluted the opposite barrel and barrel 2) 10mM H_2PtCl_6 + 10mM $CuSO_4$ + 1mM H_2SO_4 + x1000 diluted the opposite barrel. Potentials for Cu and Pt were, respectively, -1.0V and -1.16V and a bias of ±0.8V was used. The substrate is 45° tilted.*

Figure 5-12 is a SEM image of a multi-metal test. The top row alternates a Cu pillar with a Pt pillar. The second row contains two metal pillars with a Pt base and a Cu upper part. Finally, the third row contains also two metal pillars but with a Cu base and a Pt upper part. Visual difference can be appreciated between the Pt and the Cu parts of the pillar.

The Cu wires have an average of 400nm in diameter while the Pt only 270nm. However, the diameter in both metals stays stable along the structure and is reproducible pillar to pillar. It has been demonstrated in previous work in LBB that the voltage has a direct influence to pillar diameter. Therefore, in order to make more regular pillars with a smoother transition in the interface of metal change, the author recommends to decrease the printing voltage of copper. The Pt voltage should not be increased as it is working in the edge of HE.

An EDXS is required for elemental analysis and chemical characterization of the metals that have been deposited. An EDXS map was taken on the same sample as Figure 5-12.

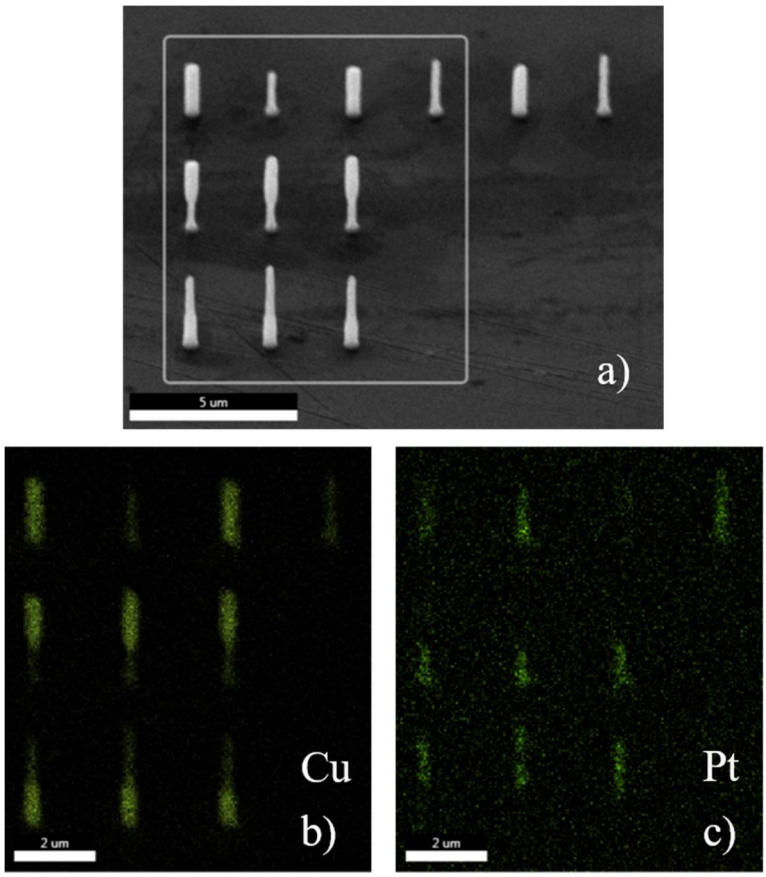

Figure 5-13. *EDXS analysis of two metal pillars test for Cu-Pt system. a) The area where EDXS was applied, SEM image with 45° tilt. b) Pixels of Cu Kα level detected. c) Pixels of Pt Lα level detected.*

The composition of each pillar is in agreement with the printing. The difference between Cu and Pt areas is clearly defined. The background of Figure 5-13c is completely scattered of Pt pixels. This is a recurrent noise error that appeared when doing the EDXS analysis of Pt. Platinum L-alpha energy level is very close to gold L-alpha energy level, 9.442 and 9.713KeV respectively as both metals are next to each other in the periodic table. The EDXS analysis used has a resolution of 126 eV, so, theoretically it should be able to differentiate between both metals. Yet, it has been found in the analysis that in some cases it confuses both metals. For the analysis of the Cu-Pt it is not a big concern because we are not printing any gold. Therefore, the gold can only be found in the substrate and that the Pt pixels detected in the substrate is noise. However, in the results of the Au-Pt system, this noise became a major issue.

In the EDXS analysis, it was found that Cu is more present in the Pt areas than Pt into Cu. Several factors can induce this result. First, that not a strong enough bias was used when depositing Pt. Second, that Cu is deposited at a lower potential causing that when Pt is

printed it can be still deposited despite the bias. Third, that Cu contamination in the opposite barrel is higher than the respective contamination of Pt (as it cannot be found when printing Cu). Hopefully, the three possible factors can be solved. Increasing the bias for the first option, decreasing the concentration of Cu in the barrels, therefore, decreasing its proportion with respect to Pt for the second factor and, finally, use a lower potential and lower bias when printing Cu so that the contamination of the opposite barrel is lower.

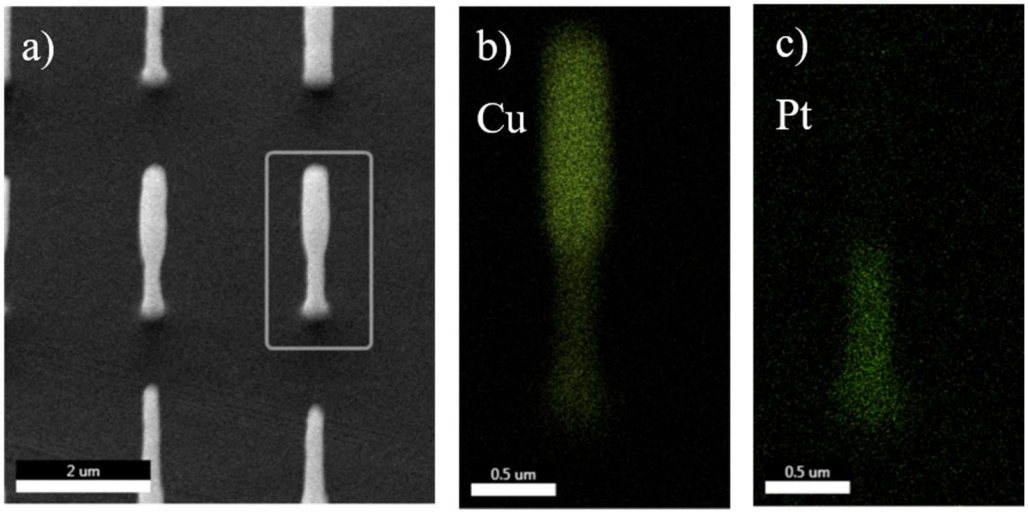

Figure 5-14. *EDXS analysis of a single pillar of Cu-Pt system. a) The area where EDXS was applied, SEM image with 45° tilt. b) Pixels of Cu Kα level detected. c) Pixels of Pt Lα level detected.*

As exposed in the last paragraph, a balance between concentrations, bias and printing voltages is needed for achieving the best performance. Take into account, though, that a strong change in these factors equilibrium can trigger other undesired results. Check Figure 5-17 where the concentration of Cu was changed as well as the biases.

A closer look was taken to one of the two metal pillars for a more precise chemical analysis. In Figure 5-14 and Figure 5-15 the results are shown.

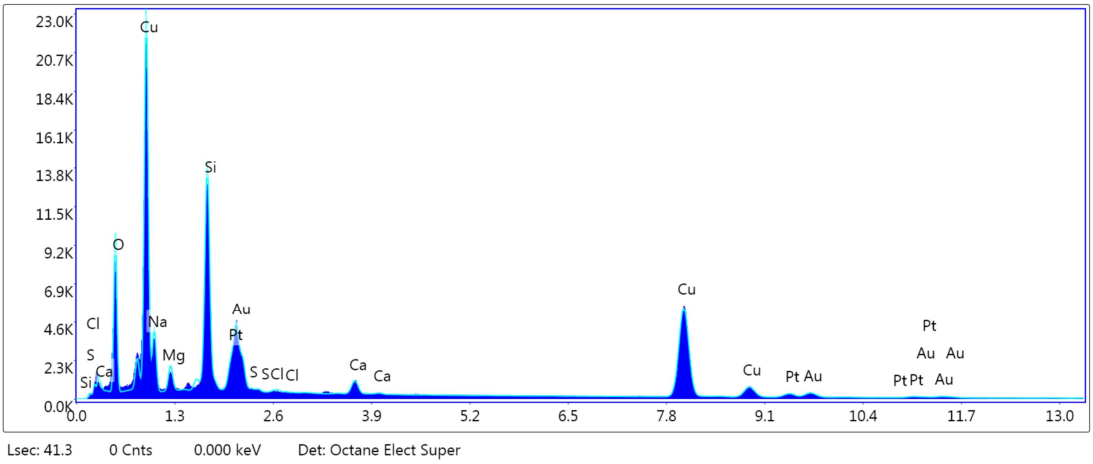

Figure 5-15. *Quantitative analysis of the EDXS in the SiK/CuK/O K/NaK phase. In the horizontal axis, the energy level is presented. In the vertical axis, the number of counts can be seen. The software detected the element for each energy peak.*

Both printed metals are present in Figure 5-15. On the one hand, two significant peaks of Cu are found which correspond to the L-alpha and K-alpha energy levels (0.928 and 8.046KeV). On the other hand, also two Pt peaks are found for the M-alpha and L-alpha levels (2.050 and 9.442KeV). The M-alpha level, however, gets confused with Au M-alpha level as the difference between Au and Pt is smaller than the EDXS resolution (Au M-alpha 2.123KeV). A lot of other elements peaks are detected in low energy levels such as Si, O, Ca and Mg. All of this elements are supposed to be part of the glass slide coated with the Ti and Au layers were the sample lays on.

5.3.1.2. Bias test results and discussions

The results of the bias test of Cu-Pt system are found in Figure 5-16. Both figures are split into two images, however, it is the same array of two rows that is divided into the left and right sides of it.

The impact of the bias was proved with this test. It can be seen how as the bias favorable to Pt increases, the amount of Cu in the pillars decreases up to a point that at +0.9/1.0V of bias almost none Cu is deposited. The dominance of Cu with these concentrations is clear, however the system is able to considerably diminish its proportion with high biases.

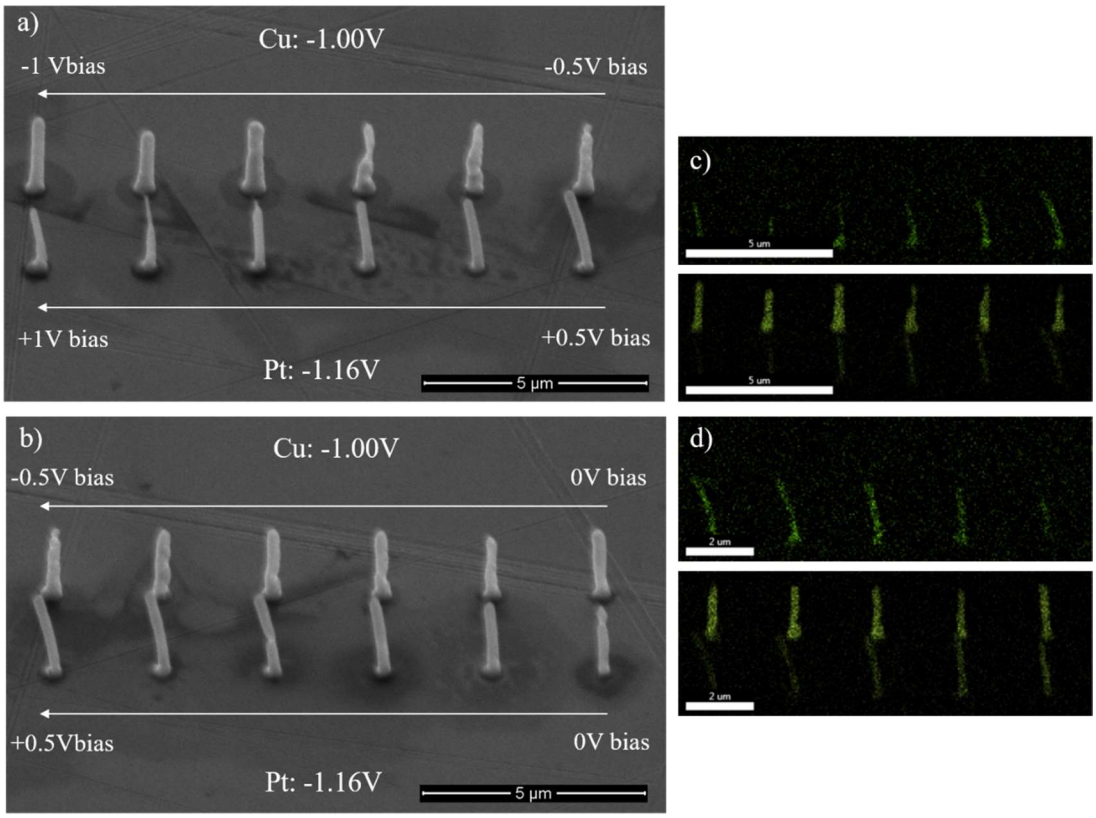

Figure 5-16. *Bias test of Cu-Pt system. a) and b) are the SEM images of the pillars with c) and d) their respective EDXS analysis. In c) and d) upper pictures are the Pt Lα level pixels and the lower picture are the Cu Kα level pixels. Electrolytes: barrel 1) 70mM Na_2SO_4 + 1mM H_2SO_4 + x1000 diluted the opposite barrel and barrel 2) 10mM H_2PtCl_6 + 10mM $CuSO_4$ + 1mM H_2SO_4 + x1000 diluted the opposite barrel.*

5.3.1.3. New concentrations for two metal pillars test

The effect of changing the electrolyte's concentrations and the bias in voltages was tested. One electrolyte of **10mM H_2PtCl_6 + 5mM $CuSO_4$ + 1mM H_2SO_4 + x1000 diluted the opposite barrel** and the other of **64mM Na_2SO_4 + 1mM H_2SO_4 + x1000 diluted the opposite barrel** were used for the two metal pillars test. A lower impact of Cu was expected as its concentration was reduced to the half. As it can be seen in Figure 5-17, Pt and Cu switched roles in comparison to Figure 5-13. In this case, Pt had a considerable more dominant deposition than Cu.

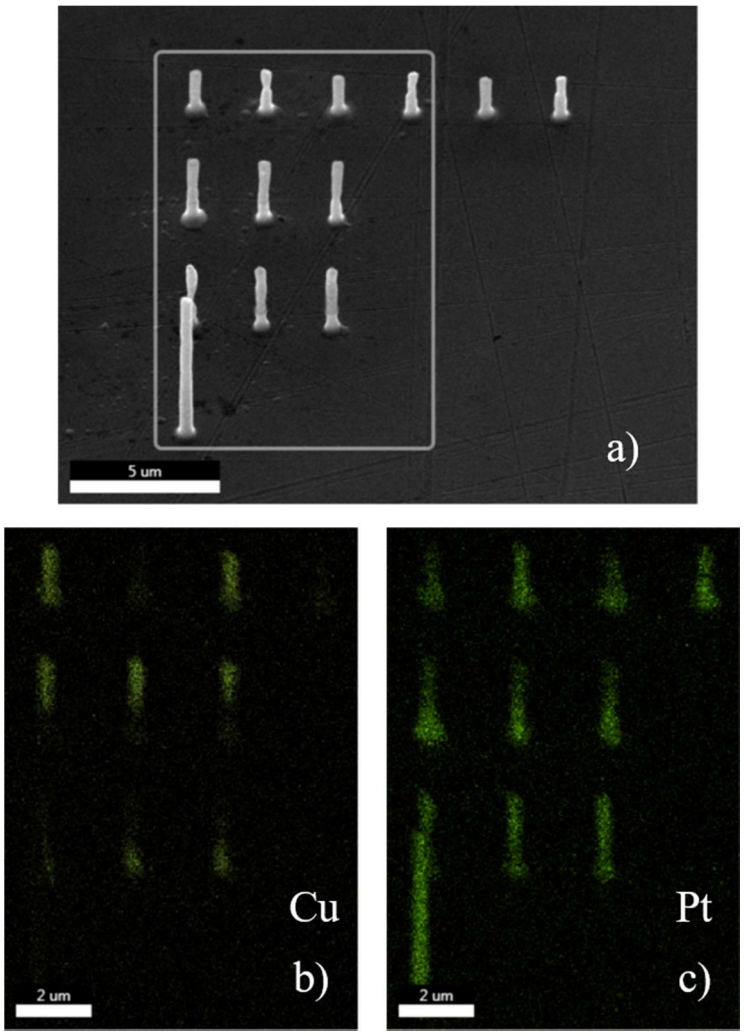

Figure 5-17. *EDXS analysis of two metal pillars test for Cu-Pt system. Electrolytes: barrel 1) 64mM Na_2SO_4 + 1mM H_2SO_4 + x1000 diluted the opposite barrel and barrel 2) 10mM H_2PtCl_6 + 5mM $CuSO_4$ + 1mM H_2SO_4 + x1000 diluted the opposite barrel. Potentials for Cu and Pt were, respectively, -1.0V and -1.16V and a bias of ±0.5V was used. a) The area where EDXS was applied, SEM image with 45° tilt. b) Pixels of Cu Kα level detected. c) Pixels of Pt Lα level detected.*

5.3.1.4. Conclusions

The correct operation of the Cu-Pt double barrel system has been proved. The system is not only able to print both metals in the same pillar one after the other but also to deposit both at the same time to create an alloy with a gradient in the chemical composition of the pillars. The proportions of the deposition of each metal can be controlled mainly through the bias as it has been seen in the bias test. However, the concentration proportion of each metal and the reduction voltage used have an impact as well, as it can be concluded from Figure 5-17.

In the experiments results of the Cu-Pt system the average printing speed of Pt has been between 50-60nm/s. From Figure 5-7 and Figure 9-1 it can be concluded that in negative bias, the deposition speed of Cu is under 10nm/s. Therefore, the Cu metal when printing Pt can be expected but it can be pushed to be an almost negligible proportion of the pillar.

5.3.2. Gold – Platinum Multi-Metal Printing

Gold-Platinum was the multi-metal system tested and developed to check the correct operation of the system for two metal with same ion polarity. Gold was chosen because of its good electrical properties, because of the similarities with platinum in the electrolyte solution (both were obtained from their chloric acids) and because of the option of printing autocatalytic nanoswimmers with a more noble and stronger metal than copper.

As seen in Figure 3-4, Au and Pt metal ions have opposite polarities. Therefore, both need to be located in opposite barrels. The chloroplatinic acid has a better conductivity than the chloroauric acid. A conductivity mismatch appeared. To solve it, initially, the same salt used in the Cu-Pt system was added to the gold barrel. However, some crystals were formed and the printing was not smooth enough. Therefore, chloroauric acid concentration was increased to even the conductivity in the platinum barrel. For the following figures, one barrel contained **10mM H_2PtCl_6 + x1000 diluted the opposite barrel** and the other contained **20mM $HAuCl_4$ + x1000 diluted the opposite barrel**. When it came to print these two metals a balance was needed between barrel's conductivity and concentration equilibrium when deciding the concentrations.

5.3.2.1. Two metal pillars test results and discussions

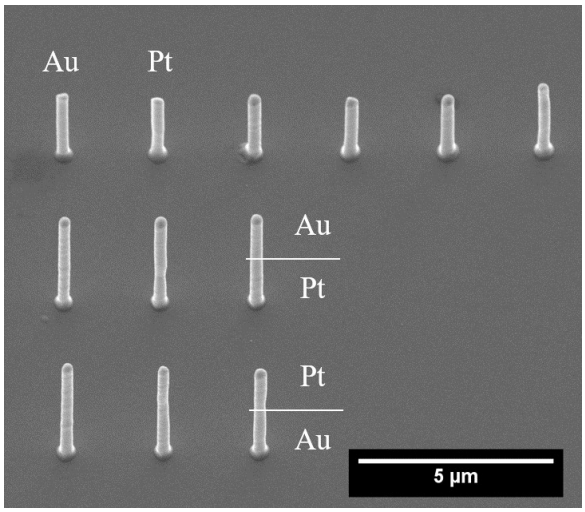

Figure 5-18. *Two metal pillars test for Au-Pt system. Potentials for Au and Pt were, respectively, -0.85V and -1.16V and a bias of ±0.6V was used. The substrate is 40° tilted.*

The two potential used for Au and Pt were -0.85V and -1.16V respectively. Figure 5-18 consists on a SEM image of a multi-metal test. The top row alternates a Au pillar with a Pt pillar. The second row contains two metal pillars with a Pt base and a Au upper part. Finally, the last row contains also two metal pillars but with a Au base and a Pt upper part. Compared with the respective picture in the Cu-Pt system, the pillars look more smooth and regular and the metal change interface is more difficult to detect. Both Au and Pt pillars have an average diameter of approximately 310nm.

An EDXS analysis was done to this sample in order to check the chemical characteristics of the printed pillars. The results of the analysis can be seen in Figure 5-19. In last chapter, noise due to the proximity of L-alpha levels of gold and platinum was not a concern. However, when it comes to print gold and platinum on top of a gold substrate, the precision of the element lecture becomes crucial and any possible confusion of the EDXS can turn into a misinterpretation of the results. This is why printing in another substrate different from the metals being deposited is an interesting matter of study.

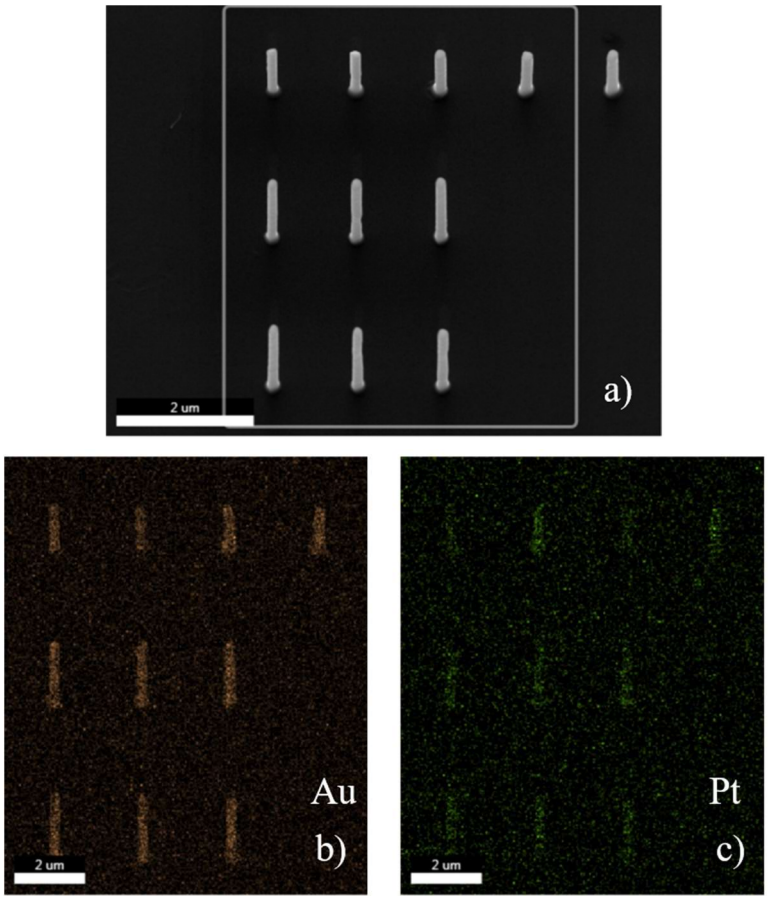

Figure 5-19. *EDXS analysis of two metal pillars test for Au-Pt system. a) The area where EDXS was applied, SEM image with 40º tilt. b) Pixels of Au Lα level detected. c) Pixels of Pt Lα level detected.*

In this test, Au dominated over Pt deposition. The intensity of Pt printing is considerably lower than gold. Anyhow, the system was able to deposit both metals. Au can be found in the whole pillar and Pt only in its expected area. Similar to the Cu-Pt case but more intensified in Au domination.

To make sure that the EDXS was not confusing both metals (as the background noise in Pt is considerable), another EDXS analysis was done in two of the pillars. In this situation, to avoid surrounding noise, punctual analysis were executed. In Figure 5-20 the results can be found. One point in each of the first two pillars of the upper row were studied. The first is expected to be full gold, the second, full platinum.

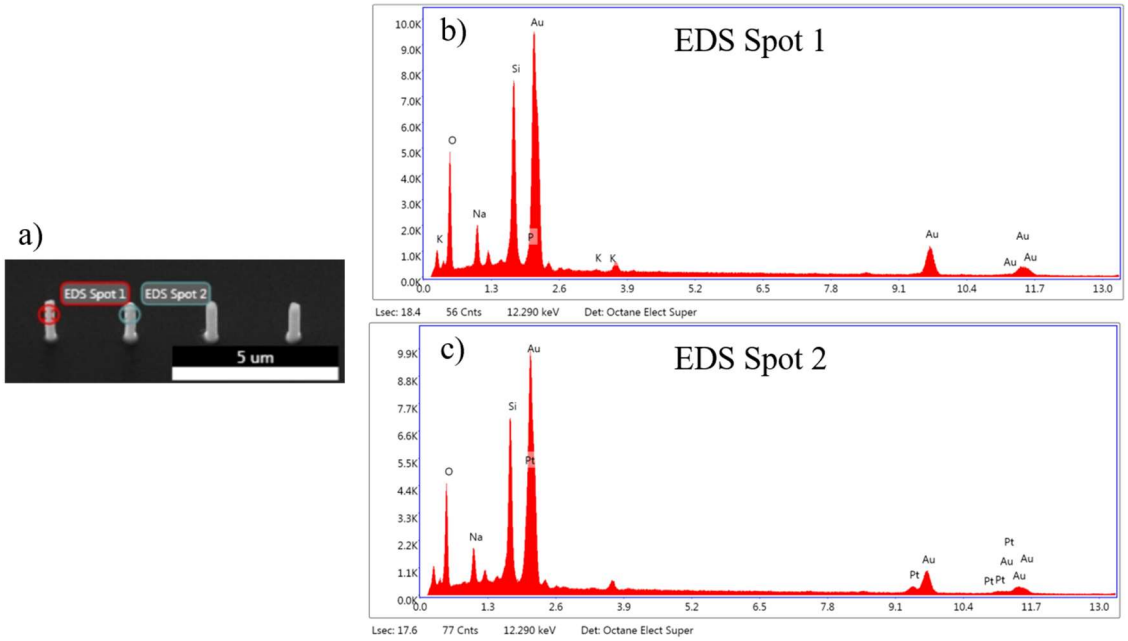

Figure 5-20. *Punctual EDXS analysis of two metal pillars test for Au-Pt system. Electrolytes: barrel 1) 20mM $HAuCl_4$ + x1000 diluted the opposite barrel 2) 10mM H_2PtCl_6 + x1000 diluted the opposite barrel. Potentials for Au and Pt were, respectively, -0.85V and -1.16V and a bias of ±0.6V was used. a) The points where EDXS was applied, SEM image with 40° tilt. b) Elemental spectrum of point 1, a gold pillar. c) Elemental spectrum of point 2, a platinum pillar.*

In the first pillar, only gold is detected (except of some elements contained by the substrate) as expected. In the second pillar, platinum and gold are both detected. However, there is no way to ensure which proportion of the gold detected is from the substrate and which is from the actual pillar.

5.3.2.2. Bias test results and discussions

The next multi-metal test that is presented is the bias test. Figure 5-21 shows the SEM image of the pillars and Figure 5-22 its EDSX analysis. In the upper row, the Au reduction potential is used with a bias favorable to its deposition. In the lower row, the Pt reduction potential and Pt favorable bias is applied.

In Figure 5-21, the pillars with closest bias to zero in both rows seem to have a different consistency. Applying zero bias allows both metals to be deposited and the mix of both metals may produce this different texture in the pillars. In Figure 5-22 it is illustrated that those pillars contain a considerable amount of both metals.

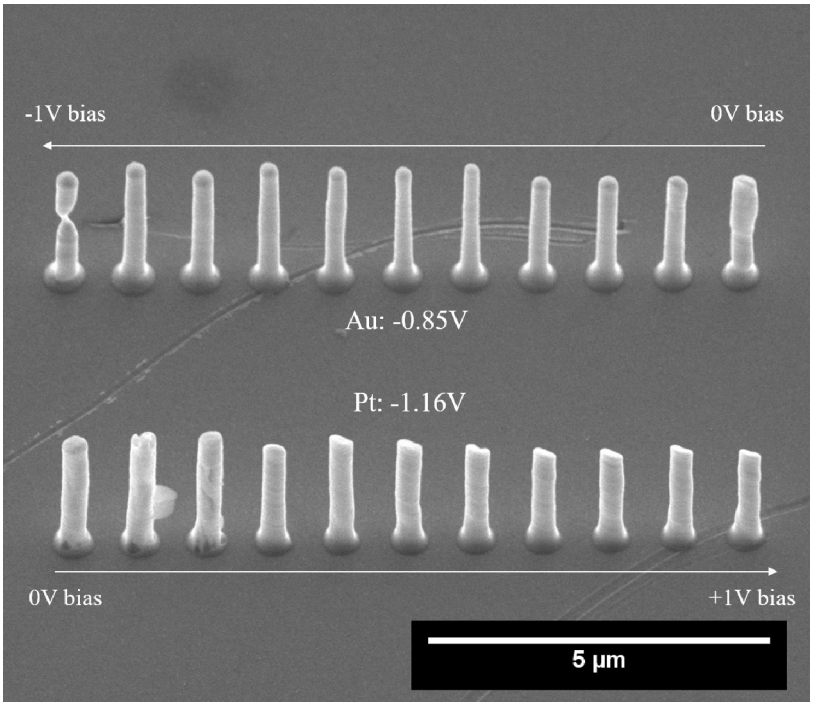

Figure 5-21. *Bias test of Au-Pt system. In the upper row, the Au reduction potential is used with a bias favorable to its deposition. In the lower row, the Pt reduction potential and Pt favorable bias is applied. Electrolytes: barrel 1) 20mM $HAuCl_4$ + x1000 diluted the opposite barrel 2) 10mM H_2PtCl_6 + x1000 diluted the opposite barrel.*

The effect of bias in metal deposition control can be clearly seen in Figure 5-22. The pillars with highest bias (±1V) are the purest of each metal and the pureness decreases as the absolute value of the bias decreases. With the highest bias used there is still some contamination of the other metal. The most probable explanation is that even when pulling away all the ions of one metal, if there is any kind of cross-contamination between barrels, the ions that have changed its barrel and have not deposited are going to be electroplated as

soon as the other metal is pushed towards the meniscus. A possible way to solve this issue is to impose a resting time when the metal is changed. During this resting time a bias between electrodes can be stablished such as that it pushed the ions of the next metal to be printed to the opposite barrel together with the ions of the last printed metal that had contaminated that barrel. Hence, the barrel of the next metal is clean of impurities and the opposite barrel is contaminated with the same metal that is going to be deposited. If it can be ensured that the contamination happens near the nozzle and that in every cycle it can be cleaned, this methodology should solve the contamination problem.

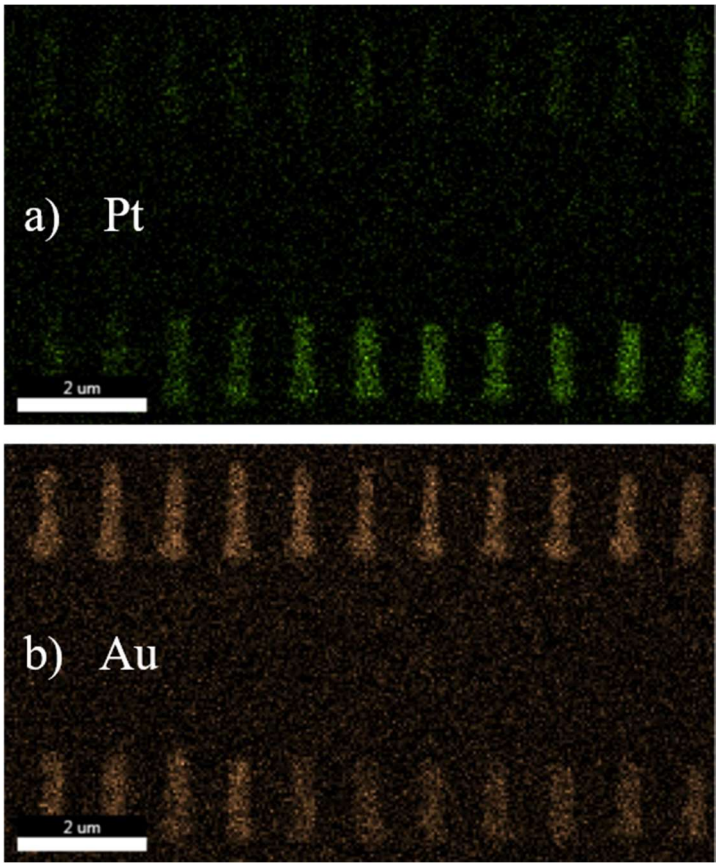

Figure 5-22. *Bias test of Au-Pt system. a) Pt Lα energy level and b) Au Lα energy level. Electrolytes: barrel 1) 20mM $HAuCl_4$ + x1000 diluted the opposite barrel 2) 10mM H_2PtCl_6 + x1000 diluted the opposite barrel.*

5.3.2.3. Conclusions

A good operation of the Au-Pt system has been proved. Therefore, the system designed for two metals with same ion polarization is feasible. The obtained results can be improved with some optimization of the concentrations and bias as discussed before. However, it would be interesting to print a single barrel pillar of each metal next to the tests in order to use it as control. This would help to quantify the actual proportions of each metal as we would be

able to compare with the control that would contain only one metal. Moreover, a new material for the substrate is needed to avoid all the noise in the background. With the new substrate, more reliable images and results are going to be obtained.

New substrate materials and combinations of them were tested to reduce the noise of the substrate: silver (Ag), chromium (Cr), carbon (C), aluminum (Al) and tungsten (W). Resistance tests and printing tests were assayed with all of them. The coating of the glass slide was realized through the sputtering of these materials. In the next table, the conductivity of each substrate is presented with respect to the metal coated, all with 30nm thick layers. Several measurements to different substrates for each material were done with a multimeter. The resistance was measured by separating the probes one cm when doing the measurement.

Carbon was discarded for poor conductivity. On aluminum and chromium, the approach was possible but the printing was unstable. Both are very reactive metals and generated an oxide layer on top that prevented the printing, Al_2O_3 for aluminum and Cr_2O_3 or CrO_2 for chromium. On tungsten the printing did not work. Finally, silver, as it is a noble metal, it had no oxidation layer in its surface before printing and because of its low resistance was a potential option to work as substrate. Silver is a good fit for EDXS analysis as its energy levels (Kα 22.163 and Lα 2.983keV) fall away gold and platinum ones.

Material	**Resistance per cm [$\Omega \cdot cm^{-1}$]**
Gold (Au)	8.4 ± 3.2*
Silver (Ag)	6.2 ± 2.9
Chromium (Cr)	104.7 ± 6.8
Aluminum (Al)	23.1 ± 2.6
Tungsten (W)	79.7 ± 5.4
Carbon (C)	100k**

Table 5-2. *Resistance substrate of different materials with 30nm thick layers.*Gold layer was actually of 25nm with 3nm of Ti underneath. **The single layer of carbon had a huge resistance and it was initially discarded, however, it was tested later with a metal layer below (with Au and Ag), in those cases it usually only increased few Ω the resistance.*

5.3.2.4. Resume of conductivity and electrolyte's concentration

This chapter contains a table resume of the concentrations and the conductivity parameters of the electrolytes used to print the multi-metal structures in this project.

	Barrel	Electrolytes and concentrations	Ions concentrations [mM]	Conductivity [S·m^{-1}]	pH
Au-Pt	1	• $HAuCl_4$: 20mM • H_2PtCl_6 : 10µM	• H^+ : 20.02 • $AuCl_4^-$: 20 • $PtCl_6^-$: 0.01	1.47	1.6
	2	• H_2PtCl_6 : 10mM • $HAuCl_4$: 20µM	• H^+ : 20.02 • $AuCl_4^-$: 0.02 • $PtCl_6^-$: 10	1.56	1.7
Cu-Pt	1	• H_2PtCl_6 : 10mM • $CuSO_4$: 10mM • H_2SO_4 : 1mM • Na_2SO_4 : 70µM	• H^+ : 22 • Cu^{2+} : 10 • $PtCl_6^-$: 10 • SO_4^{2-} : 11.07 • Na^+ : 0.14	1.90	1.7
	2	• Na_2SO_4 : 70mM • H_2SO_4 : 1mM • H_2PtCl_6 : 10µM • $CuSO_4$: 10µM	• H^+ : 2.02 • Cu^{2+} : 0.01 • $PtCl_6^-$: 0.01 • SO_4^{2-} : 71.01 • Na^+ : 140	1.87	3.2

Table 5-3. *Resume of the electrolyte's concentrations and their conductivity and acidity characteristics for each barrel and metal pair.*

5.4. Structures Release

The possibility of releasing the printed structures from the substrate had a large interest for this project. In order to obtain and use a functional nanoswimmer, which consists on a mobile element, it has to be liberated from the surface. For this reason some research was executed.

The release required a chemical process considering that mechanical release in the dimension of the structures is hard to execute and control.

5.4.1. Sacrificial Layer and Etching

Most of the literature uses sacrificial layers for structures release. A sacrificial layer is used to build the components and work as a support. Subsequently, be removed using a selective etch process that does not damage the components. For the use of multi-metal MCED technique, the sacrificial layer has to be the one were the structures are printed. The sacrificial layer develops the substrate function, therefore, it needs to accomplish two main characteristics: to be conductive enough for the printing system and to be etched smoothly. The main goal is to be able to release the structures without damaging them. For this reason,

the sacrificial layer needs to be etched faster than the structures or to be etched by a chemical that does not affect the printed materials.

Two types of etching can be used: wet and dry etching. Wet etching consists on the use of liquid-phase etchants. The sample is immersed in a bath of etchant and it leads to an isotropic, high rating and high selectivity etching. On the other hand, the dry etching consists on the use plasma-phase or gas-phase etchants. It usually has a reduced material consumption and it is anisotropic. Both of them were used for different sacrificial layers.

Several sacrificial layers were tested during the project. In the following chapters, the results of working with the different sacrificial layers are exposed

5.4.1.1. Etching glass

The first attempt was, actually, not to use a sacrificial layer, but etch the glass slide from underneath the substrate metal layer. The metal layer was scratched next to where the structures were printed. The glass etchant was supposed to etch all the glass under the metal and release the pillars and the metal layer from the glass slide. Given the fact that the metal layer is only few nm thick, it was expected to shatter into small pieces and free the structures.

The samples were submerged in different solutions of KOH (10%, 30%) at 80ºC for several hours with a stirring magnet to ensure convection of the liquid and thermal homogeneity. The system did not work. The etchant struggled to filter through the scratch and to etch under the metal layer.

5.4.1.2. Gold sacrificial layer

The next attempt was to use gold layer as a sacrificial layer. Gold layer had been used for all the multi-metal printing development. Therefore it was a well-known substrate for printing. However, gold is a noble metal difficult to etch as it is hard to dissolve. Despite this, several methods can be used [90, 91].

The most common is the use of aqua regia, a mixture of nitric acid and hydrochloric acid. Agua regia, though, also etches copper and platinum. Some authors use aqueous solutions of very toxic sodium cyanide (NaCN) or potassium cyanide (KCN) also very toxic. Because of the toxicity, this method was discarded. The gold etching method tested was the one involving iodine and iodide provided by a solution of KI (500mM used) in which the ion I^- gets reduced by an external potential.

The solubility of AuI is improved by adding KI to the solution. A three electrodes potentiostat was built. A reference electrode of carbon to control the voltage, a working electrode consisting on the substrate to be etched and a counter electrode of carbon to measure the current were employed. A voltage pulse to reduce I^- was applied. As soon as the ion got reduced, the gold started etching. The setup worked nicely, the plan was to induce the etching with a short pulse enough to etch the substrate but do not damage the structures. Copper, however was also strongly etched with this method and only platinum was able to do not get attacked. Therefore, two of the three metals that we were able to print got etched by this method and the multi-metal lost its sense.

As gold was one of the metals being printed and a new substrate was needed for improving the EDXS analysis of the structures, etching gold was discarded. However, an extra interesting gold etching method was left to be tested. It uses an alkaline thiourea solution with Na_2SO_4 and $Na_2S_2O_3$ [92]. This method is supposed to do not attack copper neither platinum.

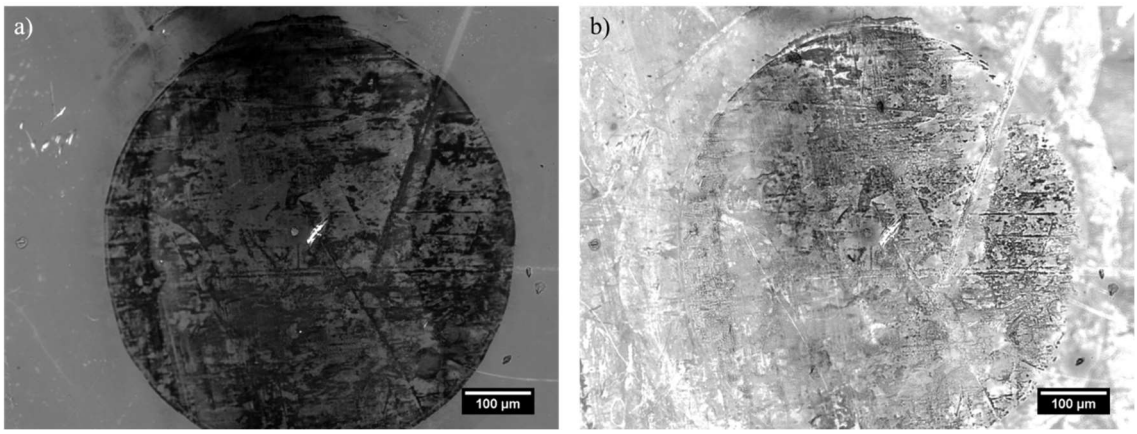

Figure 5-23. *Gold substrate of 25µm thickness with a disk of copper deposited on top. a) Before the voltage pulse, therefore, before the reduction of I^- ions and the etching. b) After a 3000ms 5V pulse. Both gold and copper have been etched equally.*

5.4.1.3. Chromium sacrificial layer

Chromium etchants are usually based on ceric ammonium nitrate $(NH_4)_2[Ce(NO_3)_6]$ with perchloric acid (HCl_4) as an optional additive. Copper and silver are strongly etched by this mixture, however, the noble metals gold and platinum are not. This is why chromium sacrificial layer was tested.

Chromium was abandoned because we were not able to print on top of it. An oxide layer was generated on the surface and the substrate conductivity decreased drastically canceling the deposition.

5.4.1.4. Carbon sacrificial layer

Because of the difficulty to find a metal etchant that did not attack the three deposited metals (Cu, Au and Pt), a non-metal sacrificial layer etched through plasma-phase was tested. Initially a single layer of 30nm of carbon was tried out, however, its resistance was too high for a correct printing. In order to reduce the resistance of the substrate, a double layer substrate was used: 25nm of gold plus 30nm of carbon on top.

We were able to print on top of the double layer substrate because the resistance of the carbon was reduced considerably thanks to the gold. To etch carbon a plasma cleaner of 18W (Harrick Plasma PDC-32G, Ithaca, NY, USA) was used. The results can be seen in the following picture.

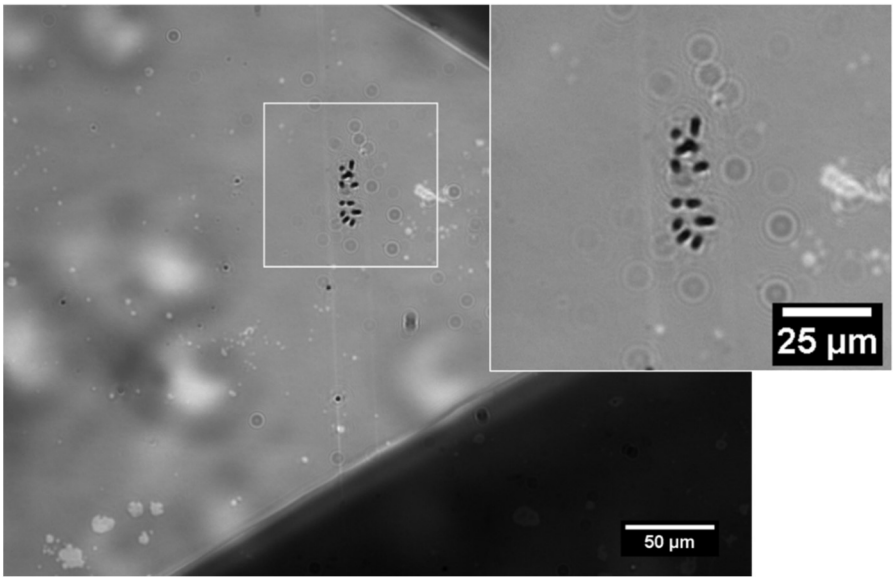

Figure 5-24. *3µm tilted gold pillars after having etched the 30nm carbon layer on top of 25nm gold layer using the plasma cleaner. The sample was for 12min inside the plasma cleaner at 18W power and a vacuum of $2 \cdot 10^{-2}$mbar.*

The carbon got usually completely etched, however, the pillars remained at the same position with a slight tilt. They kept attached to the gold layer even when they were supposed to be printed on the carbon layer.

5.4.1.5. Silver sacrificial layer

Silver is a noble metal with unique electrical properties, it has the highest electrical conductivity of all metals. It is the substrate material with lower resistance as can be seen in Table 5-2 and its corrosion in air contact is minimum. Although being also noble metal has less resistance to strong acids than platinum and gold. For its etching it needs a solution that oxidize it. From [93] which describe a method for nanoswimmers production, a solution of acid nitric (HNO_3) is used. The acid nitric attacks copper but gold and platinum are resistant to it.

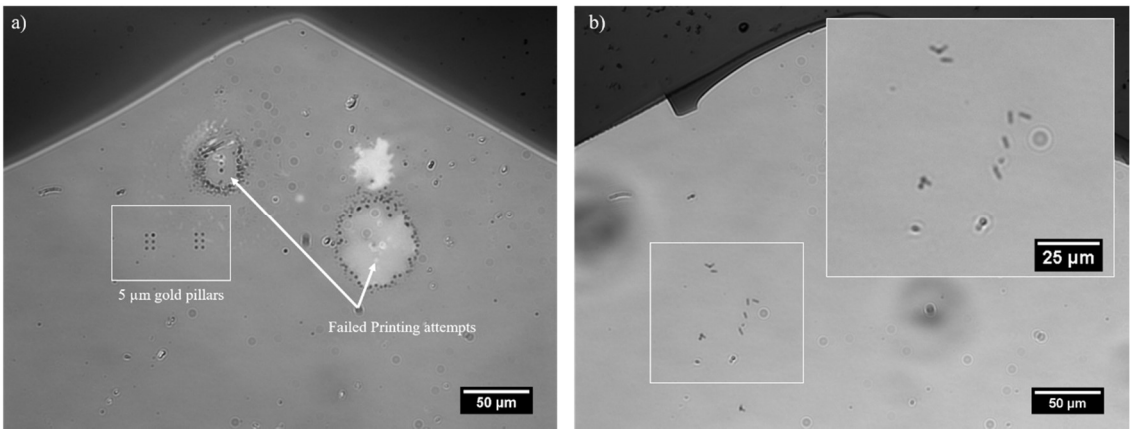

Figure 5-25. *Silver etching experiment. a) Silver substrate before being etched. b) Silver substrate after being etched with 33% HNO_3.*

In Figure 5-25 a picture of an etching experiment of a silver substrate can be found. All of the gold pillars are released from the substrate after etching. However they have been displaced from their initial position and not all of them could be found. The first printing attempts on silver were unsuccessful because the printing electrolyte of gold and platinum etched the silver substrate and any kind of deposition was achieved. Both electrolytes are strong acids with pH close to 2 which corrode the silver layer. To prevent the substrate etching by the electrolytes, the time of contact of the electrolyte with silver had to be reduced. As soon as the first layers of printing metal are deposited, the electrolyte stops having contact with the substrate and is generated only between the pillar and the nozzle. Therefore, fast initial depositions were needed. The retract speed factor (to break the meniscus in less time) and the reduction voltages (more ions flow) were increased for the first 0.6µm of the pillars. Then, the optimal parameters were set again for the rest of the pillar.

5.4.2. Microstructures confinement

Silver responded correctly as a sacrificial layer. A methodology for confining the structures once they have been released is required. There is an interest for any printed structure to maintain it in a visible area and do not let it flow away with the convection created by the wet etching. In order to impose a confinement of the structures and to protect them from the liquid flow, wells of 350µm of diameter were used. The well was mounted on top of the glass slide and then sputtered with a 30nm Ag layer. No silver could be under the well because the etchant would filter and detach the well from the glass slide and left the structures unprotected.

Initially, an approximated 60µm thick PDMS film with a hole of the desired well size was used. This material was found not be useful because it released a thin film that covered the internal area of the well. This film was not etched, as it was polymeric, and folded and wrapped the structures that stayed on top of it. In Figure 5-26, two examples of the polymeric film can be observed.

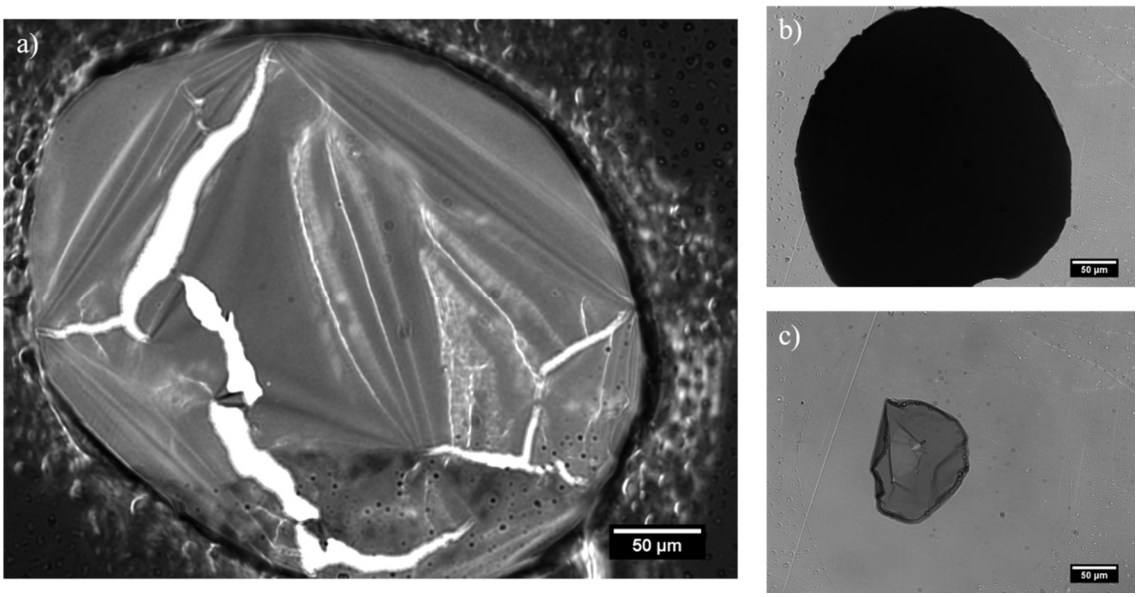

Figure 5-26. *a) PDMS well with a coating of silver being etched by 10% HNO_3. The polymeric film breaks into parts that are tensed and fold into themselves as the silver is getting etched. Several fissures can be observed. b) and c) Pictures of before and after etching with 10% HNO_3 the coated hole when the PDMS well was extracted previously.*

Another well material was needed and Scotch tape was tested. The thickness of the tape was 62.5µm (provided by the vendor). The procedure was the same as with PDMS, first attach the tape to the glass slide and then sputter the sacrificial layer. Conductivity problems arise

when printing inside the wells. The well hole was not correctly connected to the rest of the substrate. A two layer approach was taken: the Scotch tape was mounted on top of a glass slide with an already coated gold layer and then silver was sputtered on top. With this technique, all the substrate was connected through the gold layer and the structures were printed on top of silver, which can be etched, inside the well. The results can be observed in Figure 5-27.

When trying to etch the interior of the well, air bubbles used to block part of it. The etchant liquid droplets were larger than the well itself, therefore it was difficult to extend the etchant all along the well. Usually some areas next to the walls were not covered by the etchant as some air bubbles blocked them. A new technique was developed to fill the wells with etchant without any bubbles. A PDMS structure consisting on four walls 0.6mm thick and 1.8mm tall creating a closed area of 4mm x 6mm was mounted on top of the substrate confining the well (always making sure that no silver is underneath to avoid leaking when etching). The container formed by the walls was filled with ultra-pure deionized water and left it in a vacuum chamber for several minutes until all the air bubbles disappeared. Then, high concentrated etchant was added. The etchant was diluted with the already present water inside the PDMS walls, the right etchant concentration is obtained and the well is completely etched. With this technique, small amounts of chemicals are used because the liquid that the walls can contain is around 30µl.

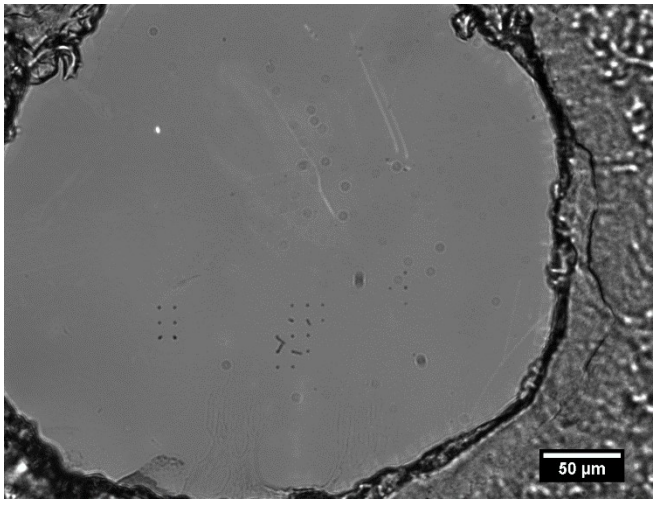

Figure 5-27. *Two metal layer substrate with a Scotch tape well and the top silver layer already etched (10% HNO_3). 5µm gold pillars can be observed. Some of them are released but the others remained attached to the gold substrate.*

Another solution was required for improving the well conductivity. A channel that connected the well to the outside was cut precisely in the tape with a blade before sputtering

silver. When the silver was sputtered on top, the channel acted as a connector between the well hole and the rest of the substrate (see Figure 5-28). Because of the reduced size of the channel (around 70µm), the well was still protecting the structures and worked the same way.

The Scotch tape well with the channel resulted to be a working solution to the confinement challenge.

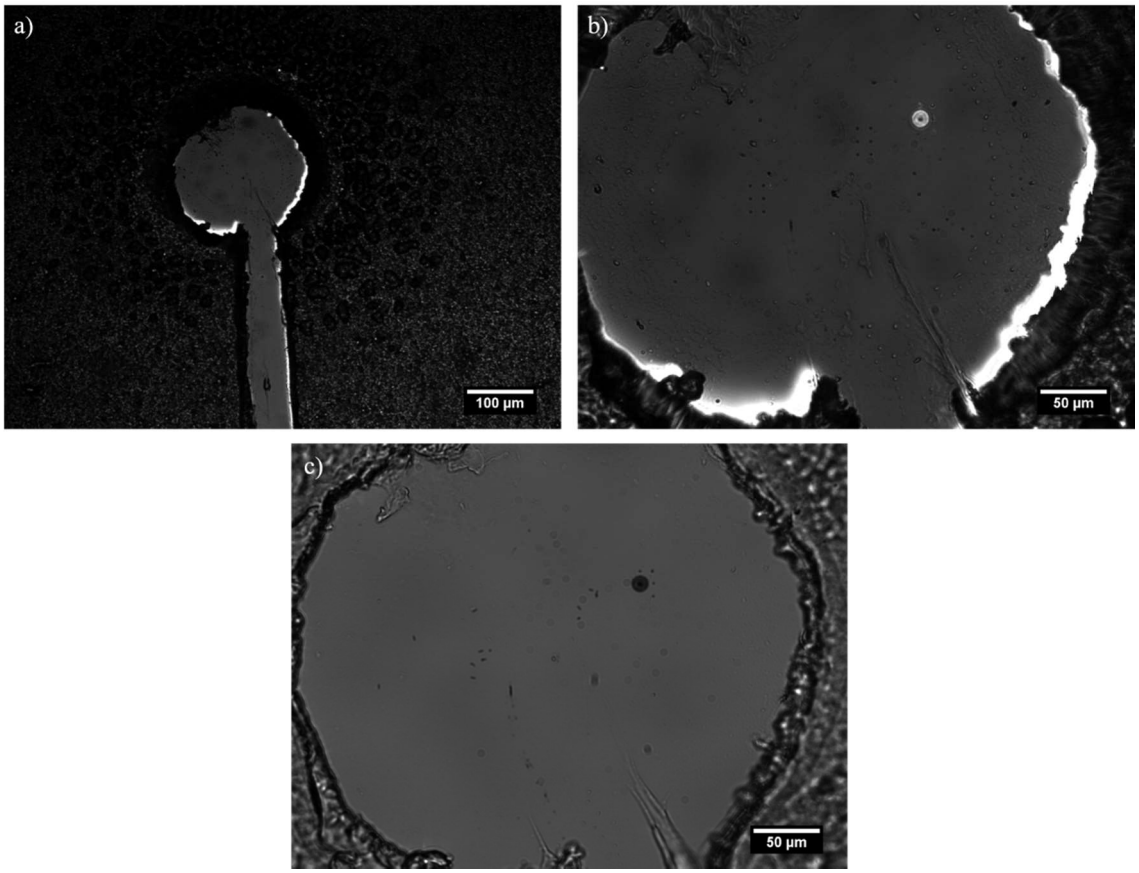

Figure 5-28. *a) Scotch tape well with 70µm channel that connects it to the substrate. b) Magnification of the same well than a) with some gold pillars printed inside. c) The well after being etched containing the released gold pillars next to their initial locations.*

6. Materials and Methods

This chapter is divided into two main sections: Materials and Methods. On one hand, the setup and materials used are exposed. On the other hand, the different protocols developed during the project are explained.

6.1. Materials

6.1.1. Printing Setup

6.1.1.1. FPGA Card

National Instruments PCIe-7846 multifunction reconfigurable Input/Output Device was used for motion and voltage control and for data acquisition. It consists of a user-programmable FPGA (Kintex-7 160T) for high performance onboard processing with maximum sampling rate (per channel) of 500kS/s. The data collection was at 2µs sample time and 256 samples per data point were taken. It was running a custom software written in LabVIEW (National Instruments, Austin TX, USA).

6.1.1.2. Variable Gain Low Noise Current Amplifier

Sensitive current measurements were carried out by a Variable Gain Low Noice Current Amplifier (DLPCA-200, FEMTO Messtechnik GmbH). It is suitable for time resolved current and charge measurements down to the µs region. Moreover, it offers variable transimpedance gain from 10^3 to 10^{11} V/A, which allowed measurement of small currents in the pico-amp range. The gain setting of 10^9 V/A was employed for the experiments. This configuration provides a 3 dB bandwidth of 50kHz and a 7µs rise time.

6.1.1.3. Positioning system

The whole setup was positioned on an optical table (I-2000 Series, Newport Corp, Irvine CA USA). The setup comprised was comprised by two stages with coarse and fine positioning one in the horizontal plane (X-Y) and the other vertical (Z). The coarse positioning system for X and Y consisted in two motorized actuators (TRB25CC model, Newport Corp, Irvine CA, USA) that provided 25mm travel with sub-micron precision. The nanopositioner mounted on top of the horizontal stage was a piezoceramic stage (Nano-BioS100, Mad City Labs Inc, Madison WI, USA) with a total range of 100µm x 100µm. The coarse positioning in Z was provided by a nanopositioner, stepper motor driven (MMP3, Mad City Labs Inc, Madison WI, USA) with 25mm of motion range. For the fine Z

positioning a high speed piezo nanopositioner was used (Nano-OP30M, Mad City Labs Inc, Madison WI, USA) with a 30µm range and a 4ms step response. For all the Mad City Labs instrumentation, controllers of the same vendor (ND3-USB163-ISS).

6.1.1.4. Visualization system

All the positioning system was mounted on top of an inverted microscope (Zeiss Axiovert M200, Carl Zeiss AG, Oberkochen, Germany). Mainly x10 and x20 magnification lens were used. It was connected to a high resolution of 1.37 Million Pixels B/W CCD digital camera (ORCA-ER Digital Camera C4742-95, Hamamatsu Photonics, Japan). The light was provided by a LED light (MWWHLP1 - 3000K, ThorLabs Inc, Newton NJ, USA) of 2000mW.

6.1.2. Chemicals

Several chemicals were used with different functions: as buffers (to ensure conductivity in the barrels and correct dissolution of the electrolytes), as printing ink (source of metal ions), as etchants (to etch substrate for structures release)…

In Table 6-1 a resume of the several chemicals used can be found.

Function	Chemical	Formula	Supplier
Printing ink	Copper (ii) sulfate pentahydrate	$CuSO_4 \cdot 5H_2O$	Sigma Aldrich
	Chloroplatinic acid	8% H_2PtCl_6	Sigma Aldrich
	Chloroauric acid	30% $HAuCl_4$	Sigma Aldrich
Buffer	Sulfuric acid	1M H_2SO_4	Merck KGaA
	Sodium sulfate	Na_2SO_4	Sigma Aldrich
Etchant	Nitric acid	100% HNO_3	Fluka Chemicals
	Cr etch 200	Alkaline etchant	Microchemicals

Table 6-1. *All chemicals used with their function, formula and supplier.*

Deionized (DI) water with a conductivity of 18.2 $M\Omega \cdot cm^{-1}$ at 25ºC was used to prepare the aqueous solutions.

6.1.3. Substrate

The semitransparent substrates used to develop multi-metal printing consisted in standard microscopy glass slides coated with 25nm Au layer on top of 3nm Ti sliced in approximately 1 cm x 1 cm pieces. All were cleaned before use with subsequent rising of acetone, isopropyl

alcohol and ultrapure water and, finally the N_2 pressure gun was used to release all the remaining liquid and particles. The substrate pieces were glued to a glass slide and connected to the lock-in amplifier using some copper tape and a low noise wire.

On the other hand, some extra steps were applied to the substrates for structures releasing. Starting from the slices of glass, a piece of Scotch tape with a hole of 350 um, done by a puncture of EMS Rapid-Core, is attached on top them. With a small blade and supported by a microscope, small channels of several tenths of microns were cut connecting the well to the rest of the substrate at glass level. Then, a 30nm layer of sputtered Ag is added. At this point, the structures can be printed inside the well created by the Scotch tape hole and the coated slice.

6.1.4. Electrode

The electrode consists in a metal wire thin enough to fit inside the pipe. Two different electrodes have been used during the project, a Ag wire of 0.25 mm of diameter and also a Pt wire of 0.125 mm of diameter were used. One end of the electrode is inside the pipette immersed in the electrolyte while the other end is connected to the system.

6.1.5. Pipettes

Two types of pipettes were used during the project: single barrel for starting printing a new metal and double barrel for implementing the multi-metal printing. The nanopipettes were fabricated by pulling two types of capillaries, double barrel (Harvard Apparatus, 30-0114, Glass Capillaries TGC150-10) and single barrel (Harvard Apparatus, 30-0044, Glass Capillaries GC120F-10), using a laser glass puller (P-2000, Sutter Instrument, USA). The double barrel glass capillaries have an initial outside diameter of 1.5 mm, a wall of 0.13 mm and a septum between barrels of 0.17 mm with a total length of 100 mm. On the other hand, the single barrel glass capillaries have an outer diameter of 1.2 mm, an inner diameter of 0.69 mm and a total length of 100 mm. The pipettes were filled with the electrolyte solutions using syringes with a micro-filler (Microfil MF34D-5 capillaries, World precision Instruments).

After having pulled the glass capillaries, the single barrel pipettes have an aperture of around 200 nm in diameter. The double barrel pipettes have an aperture of approximately 220 nm of diameter for each barrel. In Figure 3-2a a double barrel pipette aperture can be seen that can be compared with the single barrel pipette in Figure 6-1.

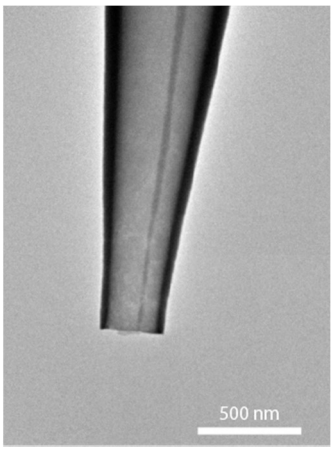

Figure 6-1. *Single barrel pipette aperture of approximately 200 nm in diameter.*

6.2. Methods and Protocols

In this chapter, the methodology followed and two protocols developed during the project are presented.

6.2.1. Printing new Metal in Single Barrel

Before printing a new metal in double barrel, it has to be studied and well-known. A protocol has been developed to start printing a new metal. Initially the single barrel printing has to be achieved before moving on the multi-metal. The steps followed are found down below.

1. **Literature reading** about the electrodeposition of the metal. A good knowledge of its ionic forms and the reduction reaction is needed. It is also important to know if the medium, such as pH or temperature, has a big impact in the deposition. Also if it generates some gas during its reduction.
2. **Find similarities to metals that already have been printed**. This will help in understanding the CV and to estimate the initial concentrations.
3. **Realize an electrochemical study** of the metal. Develop some CVs in the setup in order to find the reduction peak voltage. The concentration of the metal electrolyte is not critical in this point, from 5 to 100 mM should work. The higher concentration, the larger the peaks will be. Make sure to detect which is the metal reduction peak and when does HE start. Some materials go through different reduction reactions before depositing (such us platinum). Start with a broad voltages range to do not lose any reaction.
4. **Time to print**. Take a single barrel pipette (200 nm in aperture diameter) and fill it with the metal electrolyte. Check substrate conductivity before start printing. Take a

low concentration initially (5-20 mM), or the one recommended by literature, and print several pillars at the voltage where the highest currents appeared in the reduction peak of the CV. Set the lowest feedback threshold that the setup noise enables and then check the feedback currents that appear once the printing has finished. They should be higher than 0.5nA and lower than 3nA during the stable printing (this is an approximation and may change depending on the pipette and the material used). Module the concentration with respect to that and ensure that none clogging is taking place and that the concentration is enough to deposit the metal.

5. **Find the best printing voltage.** Once you have a concentration that works, generate a csv file with different pillars at different voltages. Starting from the peak reduction voltage, take a range of voltages higher and lower than the peak voltage using steps of 0.1V and print more than one pillar for each voltage. Then analyze the data obtained and check three main parameters: printing speed, feedback current and theoretical pillar diameter. The three parameters have to be working at the same time. Always the fastest printing is desired but when the correct and stable currents (0.5-2.5 nA) and the expected diameters are obtained. High currents usually go together with fast printing but in some cases, HE causes fake high currents. This can be detected thanks to the growing speed. Expect theoretical diameters from 150 nm to 350 nm in diameter (this factor is the less relevant as it is an approximation).
6. **Refine printing voltage**. The step 5 can be done several times with finer steps to find the ideal voltage. In some cases, decimals of V is enough (copper of gold, when the reduction peak is broad and no HE appears), other going up to hundredths of V is needed (platinum).
7. **Reproducibility and printing check**. Check reproducibility of the currents and printing speeds when the ideal voltage is found is crucial. If it is not reproducible or consistent, keep refining the printing voltage or start again at point 5.
8. **Printing**. The printing voltage and the concentration can be modified further on. Usually a range of voltages and a range of concentrations work fine together. However, it is really helpful to have a well-known and correct printing combination of the parameters to always go back if signal is lost.
9. **Structure measurements.** Finally some SEM images of the pillars can be taken in order to see that they look as expected. Also an EDX analysis is interesting to ensure that you are depositing the desired metal.

6.2.2. Printing new Metal Pair in Double Barrel

The protocol of printing a new metal pair in double barrel has a lot of similarities to the protocol of printing a new metal.

1. **Be able to print to different metals**. Before starting printing multi-metal, good knowledge of the two metals that have to be deposited is needed. The user needs to be able to print both metal apart in single barrel pipettes and to have gone through the printing a new metal in single barrel protocol.
2. **Choose double barrel system.** Depending on the polarity of both metals ions, a double barrel system has to be choose. If they have the same ion polarity, the Au-Pt system has to be used. If the ion polarity is opposite, the Cu-Pt system is the correct one.
3. **Check barrel conductivity.** It is recommended to start with the same concentration with both metal electrolytes to have an initially equilibrated system. Take the concentration used with single barrel if possible. Calculate the conductivity in each barrel and make sure it is the same for both. If it is not the same, the conductivity have to be equalized. Some inert salt such as Na_2SO_4 can be added or the concentrations of the metal salt can be increased, both in the barrel with lower conductivity. The concentration of the salt in the barrel with higher conductivity can also be decreased. The changes in the concentrations should not be drastic in order to not lose equilibrium between both barrels.
4. **Realize an electrochemical study of the electrolytes and the double barrel system.** The CVs with bias change have to be done. The user will be able to detect undesired reaction between chemicals if some peaks that did not appear in the single barrel CV appear in this one. The shift in the reduction voltage peak is also going to be detected.
5. **Time to print.** The first pillars can be printed. Fill the double barrel with the electrolytes with same conductivities. Remember to add one thousand diluted electrolyte from the opposite barrel in each barrel and to mark, somehow, which barrel contains which solution. Using slightly higher voltage than the ideal voltage in single barrel is recommended because of the bias shift. Printing alternate pillars of each metal is recommended in this first printing (alternating between 0.6/0.8 and -0.6/-0.8V in bias). The difference in printing should be notice in the data parameters when changing metal printing. The same testing criteria of single barrel can be applied in double barrel (speed, currents, and diameter).
6. **Refine printing voltage and bias.** A similar refining step can be done with the bias and the printing voltage in the double barrel system.
7. **Reproducibility and printing check**. Check reproducibility of the currents and printing speeds when the ideal voltages are found is crucial.
8. **Qualitative and quantitative measurements**. In double barrel system the SEM images and the EDX analysis are much more important than the single barrel. On

the one hand, having the SEM image of the structures is useful to adapt the voltages in order to have similar diameters in the deposition. On the other hand, the EDX analysis is basic in order to determine if you are able to print the metals as pure as you need them. If they are not as expected, some adaptations can be done. Usually, alternate metal pillars, two metal pillars and the bias range test are the structures analyzed to check the right operation of the multi-metal system.

9. **Adapting double barrel system**. If some metal is dominant over the other when printing double metal, three options can be tried to correct it: increase/decrease concentrations of the dominated/dominant electrolyte (always ensuring same conductivity in both barrels), increase/decrease printing voltages of the dominated/dominant electrolyte or to use a higher bias that enhances the deposition of the dominated electrolyte and blocks the dominant. Some reiteration between steps 6-7-8-9 may be needed until get the desired result.

7. Conclusions and Outlook

A completely novel approach to multi-metal additive manufacturing in the submicron scale was developed and studied in this thesis. The technique derives from the 3D meniscus-confined electrodeposition method. It is based on the implementation of double barrel nanopipettes with single nozzle filled with two different electrolytes connected to two electrodes that polarize both barrels and impose a reduction potential in the substrate. The technique benefits from the high resolution and simplicity of its original system. It has been seen from others studies that the MCED technique can reach up to a resolution of 10nm voxels, that prints at reasonable speeds in ambient pressures and with the resulting structures possessing excellent mechanical and electrical properties.

Multi-metal meniscus-confined electrodeposition accelerates the state of the art in multi-metal printing at micro- and nanoscale. It offers direct 3D printing of additively deposited metals with control in the local printed chemistry. It provides on-the-fly variations of the printed chemistry ranging from portions controlled alloys to almost pure metal.

Excellent performance of the technique has been demonstrated for three metals combined in pairs (Cu-Pt and Au-Pt). Although the system was tested for only three metals, the methodology can be extended to any other pair of metals as the two systems studied can be extrapolated to other metal pairs. Moreover, the system has potential to evolve to a more complex system to print more than two metals together. If we operate with multi-barrel pipettes, we can work with several electrolytes. Setting the correct potentials and biases between the barrels and managing all the factors studied in this thesis, more than two metals could be printed. Furthermore, a theoretical exercise has been done for printing three metals in a double barrel setup. If we combine Cu and Pt in one barrel and Au in the other, Cu and Au would compete to print simultaneously. In order to unbalance the situation and to be able to print only one at a time, the concentration of the metal with a higher reduction potential should be increased (Cu). When printing at low potentials, only one of the two metals deposits correctly (Au). Then, when printing at high potentials both deposit but the one with higher concentration would dominate over the other.

The project initiated with the printing of new materials employing the MCED setup. Copper and platinum deposition was studied. Copper was found to have a smooth deposition whereas platinum, as it is an excellent catalyst for hydrogen evolution, its deposition required a deeper analysis. Subsequently, the multi-metal MCED system was developed and studied for these two metals (Cu-Pt). Several factors were found to be crucial for the right operation of the system and some of them were interconnected: barrels' polarization controlled by the

bias in potentials, cathode potential, barrels' conductivity, avoidance of hydrogen evolution, electrolytes' concentrations, electrodes' material and correct election of printing program parameters. The next step consisted of developing the Au-Pt system and checking that all the hypothesis and factors analyzed with Cu-Pt also worked. The results of the two systems tests showed a promising potential. However, there is still room for improvement and optimization for a perfect operation in both systems. Not in the methodology but in the utilization (electrolytes' concentrations and potentials). Several solutions were proposed in the results and discussion section.

In the last part of the thesis, we tested a set of cathode materials in order to find a variant for gold substrate and we also evaluated several etching possibilities of different materials. The study of material etching can be used when using one of the printed metals as support material for complex 3D structures. Moreover, we developed a methodology for the release of the multi-metal printed structures. The methodology allowed a free-damage release for the structures, ensured their confinement in a reduced area and allowed a continuous tracking of all the deposited features. The releasing methodology was implemented to be used for further research in nanoswimmers [94, 95, 96]. A functional printed element was desired to be built and tested with the new technique. The metals we worked with were ideal for autocatalytic nanoswimmers of Au-Pt or Cu-Pt that could be used for fast drug delivery [97].

The multi-metal MCED technique unlocks the avenues for a broad range of chemically designed 3D devices and materials. This can culminate in uncountable small-scale applications in several fields such as electronics [5, 58], optics, sensors and actuators [94], energy storage in microbatteries [14, 98], 4D printing or micro- and nanoscale robotics.

8. References

1 KEATING, Steven J., et al. Toward site-specific and self-sufficient robotic fabrication on architectural scales. *Science Robotics*, 2017, 2.5: eaam8986.

2 GIBSON, Ian, et al. Additive manufacturing technologies. New York: Springer, 2014.

3 THOMPSON, Mary Kathryn, et al. Design for Additive Manufacturing: Trends, opportunities, considerations, and constraints. *CIRP annals*, 2016, 65.2: 737-760.

4 KANG, Hyun-Wook, et al. A 3D bioprinting system to produce human-scale tissue constructs with structural integrity. *Nature biotechnology*, 2016, 34.3: 312-319.

5 YI, Zhiran, et al. Vertical, capacitive microelectromechanical switches produced via direct writing of copper wires. *Microsystems & nanoengineering*, 2016, 2.1: 1-7.

6 O'DONNELL, John; KIM, Myungsun; YOON, Hwan-Sik. A review on electromechanical devices fabricated by additive manufacturing. *Journal of Manufacturing Science and Engineering*, 2017, 139.1.

7 JOHLIN, Eric, et al. Broadband highly directive 3D nanophotonic lenses. *Nature communications*, 2018, 9.1: 1-8.

8 IVANOVA, Olga; WILLIAMS, Christopher; CAMPBELL, Thomas. Additive manufacturing (AM) and nanotechnology: promises and challenges. *Rapid Prototyping Journal*, 2013.

9 O'BRIEN, J. L., et al. Towards the fabrication of phosphorus qubits for a silicon quantum computer. *Physical Review B*, 2001, 64.16: 161401.

10 XIANG, Zhuolin; LIU, Jingquan; LEE, Chengkuo. A flexible three-dimensional electrode mesh: An enabling technology for wireless brain–computer interface prostheses. *Microsystems & Nanoengineering*, 2016, 2.1: 1-8.

11 MOSER, H. O., et al. Terahertz response of a microfabricated rod–split-ring-resonator electromagnetic metamaterial. *Physical review letters*, 2005, 94.6: 063901.

12 DONG, Liang, et al. A microfabrication approach for making metallic mechanical metamaterials. *Materials & Design*, 2018, 160: 147-168.

13 KIM, Heungsoo; AUYEUNG, Raymond CY; PIQUÉ, Alberto. Laser-printed thick-film electrodes for solid-state rechargeable Li-ion microbatteries. *Journal of power sources*, 2007, 165.1: 413-419.

14 SUN, Ke, et al. 3D printing of interdigitated Li-Ion microbattery architectures. *Advanced materials*, 2013, 25.33: 4539-4543.

15 LUO, Jun, et al. Printing Functional 3D Microdevices by Laser-Induced Forward *Transfer. Small*, 2017, 13.9: 1602553.

16 QU, Jingyuan, et al. Micro-structured two-component 3D metamaterials with negative thermal-expansion coefficient from positive constituents. *Scientific reports*, 2017, 7: 40643.

17 SKYLAR-SCOTT, Mark A.; GUNASEKARAN, Suman; LEWIS, Jennifer A. Laser-assisted direct ink writing of planar and 3D metal architectures. *Proceedings of the National Academy of Sciences*, 2016, 113.22: 6137-6142.

18 ZENOU, Michael; SA'AR, Amir; KOTLER, Zvi. Laser transfer of metals and metal alloys for digital microfabrication of 3D objects. *Small*, 2015, 11.33: 4082-4089.

19 BEHROOZFAR, A. et al. Microscale 3D printing of nanotwinned copper. *Advanced Materials* 30, 1705107 (2018).

20 SURYAVANSHI, Abhijit P.; YU, Min-Feng. Electrochemical fountain pen nanofabrication of vertically grown platinum nanowires. *Nanotechnology*, 2007, 18.10: 105305.

21 SURYAVANSHI, Abhijit P.; YU, Min-Feng. Probe-based electrochemical fabrication of freestanding Cu nanowire array. *Applied Physics Letters*, 2006, 88.8: 083103.

22 SURYAVANSHI, Abhijit. *Meniscus controlled three-dimensional nanofabrication*. University of Illinois at Urbana-Champaign, 2007.

23 SUGIOKA, Koji; CHENG, Ya. Femtosecond laser three-dimensional micro-and nanofabrication. *Applied physics reviews*, 2014, 1.4: 041303.

24 HOHMANN, Judith K., et al. Three-Dimensional μ-Printing: An Enabling Technology. *Advanced Optical Materials*, 2015, 3.11: 1488-1507.

25 GAILEVIČIUS, Darius, et al. Additive-manufacturing of 3D glass-ceramics down to nanoscale resolution. *Nanoscale Horizons*, 2019, 4.3: 647-651.

26 VAZIN, Tandis; SCHAFFER, David V. Engineering strategies to emulate the stem cell niche. *Trends in biotechnology*, 2010, 28.3: 117-124.

27 MARUO, Shoji; INOUE, Hiroyuki. Optically driven micropump produced by three-dimensional two-photon microfabrication. *Applied Physics Letters*, 2006, 89.14: 144101.

28 SUN, Hong-Bo; MATSUO, Shigeki; MISAWA, Hiroaki. Three-dimensional photonic crystal structures achieved with two-photon-absorption photo-polymerization of resin. *Applied physics letters*, 1999, 74.6: 786-788.

29 GANSEL, Justyna K., et al. Gold helix photonic metamaterial as broadband circular polarizer. *Science*, 2009, 325.5947: 1513-1515.

30 ZEESHAN, Muhammad A., et al. Hybrid helical magnetic microrobots obtained by 3D template-assisted electrodeposition. *Small*, 2014, 10.7: 1284-1288.

31 HIRT, Luca, et al. Additive manufacturing of metal structures at the micrometer scale. *Advanced Materials*, 2017, 29.17: 1604211.

32 AHN, Bok Y., et al. Omnidirectional printing of flexible, stretchable, and spanning silver microelectrodes. *Science*, 2009, 323.5921: 1590-1593.

33 GALLIKER, Patrick, et al. Direct printing of nanostructures by electrostatic autofocussing of ink nanodroplets. *Nature communications*, 2012, 3.1: 1-9.

34 GALLIKER, P.; SCHNEIDER, J.; POULIKAKOS, D. Dielectrophoretic bending of directly printed free-standing ultra-soft nanowires. *Applied Physics Letters*, 2014, 104.7: 073105.

35 AN, Byeong Wan, et al. High-resolution printing of 3D structures using an electrohydrodynamic inkjet with multiple functional inks. *Advanced materials*, 2015, 27.29: 4322-4328.

36 TAKAI, Takanari; NAKAO, Hidenobu; IWATA, Futoshi. Three-dimensional microfabrication using local electrophoresis deposition and a laser trapping technique. *Optics express*, 2014, 22.23: 28109-28117.

37 KUZNETSOV, A. I.; KIYAN, R.; CHICHKOV, B. N. Laser fabrication of 2D and 3D metal nanoparticle structures and arrays. *Optics express*, 2010, 18.20: 21198-21203.

38 VISSER, Claas Willem, et al. Toward 3D printing of pure metals by laser-induced forward transfer. *Advanced materials*, 2015, 27.27: 4087-4092.

39 ZENOU, M.; SA'AR, A.; KOTLER, Z. Laser jetting of femto-liter metal droplets for high resolution 3D printed structures. *Scientific reports*, 2015, 5.1: 1-10.

40 ZENOU, Michael; SA'AR, Amir; KOTLER, Zvi. Laser transfer of metals and metal alloys for digital microfabrication of 3D objects. *Small*, 2015, 11.33: 4082-4089.

41 ISHIKAWA, Atsushi; TANAKA, Takuo. Two-Photon Fabrication of Three-Dimensional Metallic Nanostructures for Plasmonic Metamaterials. *Journal of Laser Micro/Nanoengineering,* 2012, 7.1.

42 FAN, Guanghua, et al. Mechanism for the photoreduction of poly (vinylpyrrolidone) to HAuCl4 and the dominating saturable absorption of Au colloids. *Physical Chemistry Chemical Physics*, 2016, 18.13: 8993-9004.

43 STELLACCI, Francesco, et al. Laser and electron-beam induced growth of nanoparticles for 2D and 3D metal patterning. *Advanced Materials*, 2002, 14.3: 194-198.

44 BOTMAN, A.; MULDERS, J. J. L.; HAGEN, C. W. Creating pure nanostructures from electron-beam-induced deposition using purification techniques: a technology perspective. *Nanotechnology*, 2009, 20.37: 372001.

45 UTKE, Ivo; MOSHKALEV, Stanislav; RUSSELL, Phillip (ed.). Nanofabrication using focused ion and electron beams: principles and applications. *Oxford University Press*, 2012.

46 PORRATI, F., et al. Fabrication and electrical transport properties of binary Co-Si nanostructures prepared by focused electron beam-induced deposition. *Journal of Applied Physics*, 2013, 113.5: 053707.

47 PORRATI, F., et al. Room temperature L10 phase transformation in binary Co-Pt nanostructures prepared by focused electron beam induced deposition. *Nanotechnology*, 2012, 23.18: 185702.

48 PORRATI, F., et al. Fabrication of FeSi and Fe3Si compounds by electron beam induced mixing of [Fe/Si] 2 and [Fe3/Si] 2 multilayers grown by focused electron beam induced deposition. *Journal of Applied Physics*, 2016, 119.23: 234306.

49 HIRT, Luca, et al. Template-free 3D microprinting of metals using a force-controlled nanopipette for layer-by-layer electrodeposition. *Advanced materials*, 2016, 28.12: 2311-2315.

50 SEOL, Seung Kwon, et al. Electrodeposition-based 3D printing of metallic microarchitectures with controlled internal structures. *Small*, 2015, 11.32: 3896-3902.

51 MCKELVEY, Kim; O'CONNELL, Michael A.; UNWIN, Patrick R. Meniscus confined fabrication of multidimensional conducting polymer nanostructures with scanning electrochemical cell microscopy (SECCM). *Chemical Communications*, 2013, 49.29: 2986-2988.

52 MOMOTENKO, Dmitry, et al. Write–read 3D patterning with a dual-channel nanopipette. *ACS nano*, 2016, 10.9: 8871-8878.

53 CHEN, Mojun, et al. Meniscus-on-Demand Parallel 3D Nanoprinting. *ACS nano*, 2018, 12.5: 4172-4177.

54 REISER, Alain, et al. Multi-metal electrohydrodynamic redox 3D printing at the submicron scale. *Nature communications*, 2019, 10.1: 1-8.

55 BAGOTSKY, V., 2006. Fundamentals of Electrochemistry. Hoboken, N.J.: Wiley-Interscience.

56 PAUNOVIC M. and Schlesinger M., Fundamentals of Electrochemical Deposition. New York: John Wiley & Sons, 1998.

57 HU, Jie. *Interfacial physics in meniscus-confined electrodeposition and its applications for fabricating electronic structures*. 2011. PhD Thesis. University of Illinois at Urbana-Champaign.

58 HU, Jie; YU, Min-Feng. Meniscus-confined three-dimensional electrodeposition for direct writing of wire bonds. *Science*, 2010, 329.5989: 313-316.

59 LIN, Yen-Po; ZHANG, Yong; YU, Min-Feng. Parallel process 3D metal microprinting. *Advanced Materials Technologies*, 2019, 4.1: 1800393.

60 CHEN, Chiao-Chen; ZHOU, Yi; BAKER, Lane A. Scanning ion conductance microscopy. *Annual Review of Analytical Chemistry*, 2012, 5: 207-228.

61 HANSMA, P. K., et al. The scanning ion-conductance microscope. *Science*, 1989, 243.4891: 641-643.

62 MCKELVEY, Kim, et al. Nanopipettes as a tool for single nanoparticle electrochemistry. *Current Opinion in Electrochemistry*, 2017, 6.1: 4-9.

63 MORRIS, Celeste A.; FRIEDMAN, Alicia K.; BAKER, Lane A. Applications of nanopipettes in the analytical sciences. *Analyst*, 2010, 135.9: 2190-2202.

64 AARONSON, Barak DB, et al. Scanning electrochemical cell microscopy: mapping, measuring, and modifying surfaces and interfaces at the nanoscale. *Nanoelectrochemistry*. CRC Press, 2015. p. 668-707.

65 KANG, Minkyung, et al. Frontiers in nanoscale electrochemical imaging: faster, multifunctional, and ultrasensitive. *Langmuir*, 2016, 32.32: 7993-8008.

66 PERRY, David, et al. Characterization of nanopipettes. *Analytical chemistry*, 2016, 88.10: 5523-5530.

67 ITO, So; IWATA, Futoshi. Nanometer-scale deposition of metal plating using a nanopipette probe in liquid condition. *Japanese Journal of Applied Physics*, 2011, 50.8S3: 08LB15.

68 IWATA, F., et al. Nanometre-scale deposition of colloidal Au particles using electrophoresis in a nanopipette probe. *Nanotechnology*, 2007, 18.10: 105301.

69 IWATA, Futoshi; METOKI, Junya. Microelectrophoresis deposition using a nanopipette for three-dimensional structures. In: 2014 *International Conference on Manipulation, Manufacturing and Measurement on the Nanoscale* (3M-NANO). IEEE, 2014. p. 304-307.

70 MÜLLER, A. D.; MÜLLER, F.; HIETSCHOLD, M. Localized electrochemical deposition of metals using micropipettes. *Thin Solid Films*, 2000, 366.1-2: 32-36.

71 BROWN, K. T.; FLAMING, D. G. New microelectrode techniques for intracellular work in small cells. *Neuroscience*, 1977, 2.6: 813-827.

72 ALLEN, J. Bard; LARRY, R. Faulkner. Electrochemical methods fundamentals and applications. *John Wiley & Sons,* 2001.

73 ELGRISHI, Noémie, et al. A practical beginner's guide to cyclic voltammetry. *Journal of Chemical Education*, 2018, 95.2: 197-206.

74 HEINZE, Jürgen. Cyclic voltammetry—"electrochemical spectroscopy". New analytical methods (25). *Angewandte Chemie International Edition in English*, 1984, 23.11: 831-847.

75 NICHOLSON, Richard Selindh; SHAIN, Irving. Theory of stationary electrode polarography. Single scan and cyclic methods applied to reversible, irreversible, and kinetic systems. *Analytical chemistry*, 1964, 36.4: 706-723.

76 PARK, Myounggu, et al. A review of conduction phenomena in Li-ion batteries. *Journal of Power Sources*, 2010, 195.24: 7904-7929.

77 DIFFUSION CUSSLER, E. L. Mass transfer in fluid systems. 1984.

78 WILKINSON, David S. Mass transport in solids and fluids. *Cambridge university press*, 2000.

79 CONWAY, B. E.; TILAK, B. V. Interfacial processes involving electrocatalytic evolution and oxidation of H2, and the role of chemisorbed H. *Electrochimica Acta*, 2002, 47.22-23: 3571-3594.

80 DJOKIC, Stojan S. Electrodeposition: theory and practice. Springer Science & Business Media, 2010.

81 DUBOUIS, Nicolas; GRIMAUD, Alexis. The hydrogen evolution reaction: from material to interfacial descriptors. *Chemical Science*, 2019, 10.40: 9165-9181.

82 ZERADJANIN, Aleksandar R., et al. What is the trigger for the hydrogen evolution reaction?–towards electrocatalysis beyond the Sabatier principle. *Physical Chemistry Chemical Physics*, 2020, 22.16: 8768-8780.

83 LASIA, A. Hydrogen evolution reaction. Handbook of fuel cells, 2010.

84 KAUFMAN, G. S. Inorganic Syntheses, Vol. 9, edited by SY Tyree Jr. 1967.

85 CHEN, Shengli; KUCERNAK, Anthony. Electrodeposition of platinum on nanometer-sized carbon electrodes. *The Journal of Physical Chemistry* B, 2003, 107.33: 8392-8402.

86 HILL, Adam C., et al. Effect of Pb (II) on the morphology of platinum electrodeposited on highly oriented pyrolytic graphite. *Langmuir*, 1999, 15.11: 4005-4010.

87 YADAV, Jyotiprakash B.; CHAE, Sang-Youn; JOO, Oh-Shim. Study of pH dependent Pt electrodeposition for hydrogen production in PV assisted water electrolysis system. *Journal of the Electrochemical Society*, 2011, 158.7: E73.

88 FLETCHER, Augustus; MORIARTY, William L. Gold electroplating bath and method of making the same. U.S. Patent No 4,168,214, 1979.

89 HAO, Rui; ZHANG, Bo. Nanopipette-based electroplated nanoelectrode. *Analytical chemistry*, 2016, 88.1: 614-620.

90 GREEN, T. A. Gold etching for microfabrication. *Gold bulletin*, 2014, 47.3: 205-216.

91 XIA, Younan, et al. A selective etching solution for use with patterned self-assembled monolayers of alkanethiolates on gold. *Chemistry of materials*, 1995, 7.12: 2332-2337

92 CHAI, Liyuan, et al. Study on selective dissolution of gold in alkaline thiourea media. *Journal of Central South University of Technology*, 1997, 4.2: 79-83.

93 LI, Jinxing, et al. Template electrosynthesis of tailored-made helical nanoswimmers. *Nanoscale*, 2014, 6.16: 9415-9420.

94 LIU, Ran; SEN, Ayusman. Autonomous nanomotor based on copper–platinum segmented nanobattery. *Journal of the American Chemical Society*, 2011, 133.50: 20064-20067.

95 OU, Juanfeng, et al. Micro-/Nanomotors toward Biomedical Applications: The Recent Progress in Biocompatibility. *Small*, 2020, 1906184.

96 SÁNCHEZ, Samuel; SOLER, Lluís; KATURI, Jaideep. Chemically powered micro-and nanomotors. *Angewandte Chemie International Edition*, 2015, 54.5: 1414-1444.

97 KAGAN, Daniel, et al. Rapid delivery of drug carriers propelled and navigated by catalytic nanoshuttles. *Small*, 2010, 6.23: 2741-2747.

98 EDSTRÖM, Kristina, et al. Electrodeposition as a tool for 3D microbattery fabrication. *Electrochemical Society Interface*, 2011, 20.2: 41.

9. Appendix

9.1. Picture of negative bias test

The result of the test of the negative bias using the same nanopipette as in Figure 5-7 can be seen.

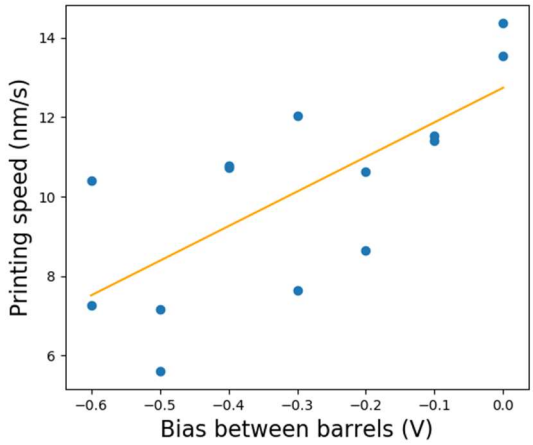

Figure 9-1. *Speed of Cu pillar deposition with respect to the negative applied bias between barrels. The linear regression of the plot has a R^2 of 0.51.*

When the printing speed is under 10 nm/s it can be considered that the deposition is almost inexistent as the system becomes really unstable.